LOYOLA UNIVERSITY CHICAGO 1870 AD · MAJOREM · DEI · GLORIAM
eCOMMONS

Loyola University Chicago
Loyola eCommons

Master's Theses | Theses and Dissertations

2022

Rapid Radiation of Zeiformes Revealed Through Comparison of Jaw Morphologies

Jeffrey Peters

Follow this and additional works at: https://ecommons.luc.edu/luc_theses

 Part of the Biology Commons

Recommended Citation

Peters, Jeffrey, "Rapid Radiation of Zeiformes Revealed Through Comparison of Jaw Morphologies" (2022). *Master's Theses*. 4462.
https://ecommons.luc.edu/luc_theses/4462

This Thesis is brought to you for free and open access by the Theses and Dissertations at Loyola eCommons. It has been accepted for inclusion in Master's Theses by an authorized administrator of Loyola eCommons. For more information, please contact ecommons@luc.edu.

This work is licensed under a Creative Commons Attribution-Noncommercial-No Derivative Works 3.0 License.
Copyright © 2022 Jeffrey Peters

LOYOLA UNIVERSITY CHICAGO

RAPID RADIATION OF ZEIFORMES REVEALED THROUGH COMPARISON OF JAW MORPHOLOGIES

A THESIS SUBMITTED TO

THE FACULTY OF THE GRADUATE SCHOOL

IN CANDIDACY FOR THE DEGREE OF

MASTER OF SCIENCE

PROGRAM IN BIOLOGY

BY

JEFFREY W. PETERS

CHICAGO, IL

MAY 2023

Copyright by Jeffrey Peters, 2023
All rights reserved.

ACKNOWLEDGMENTS

This work would not have been possible without the assistance of the members of the Grande Lab. Most importantly, I want to thank Dr. Terry Grande for being a research mentor, professor, and friend for the past eight years. She took me in as an undergraduate student when I was starting my Junior year at Loyola University Chicago, which is where I started working with zeiform fishes. I am forever grateful for that research experience, which led me to pursue research at the graduate level in her lab. Dr. Mark Wilson was a tremendous help with all my thesis figures and helped me with improving my grammar and writing skills. To Dr. Terry Grande and Dr. Mark Wilson, thank you so much for welcoming me into your lab many years ago; this thesis would truly not have been possible without your help and efforts. I am forever grateful for your patience and wisdom during this process.

Thank you to the Loyola Biology Department. Dr. Marty Berg and Dr. Thom Sanger were valuable members of my committee. They were great resources for me inside and outside of the classroom, and this thesis would not be possible without them. My first two years were financially supported by the Graduate School and the remaining time was supported by employment within the Biology Department as adjunct faculty teaching introductory biology labs. I could not have done this without the financial support and opportunity, so thank you. I also want to thank Audrey Berry and Virginia Lorenzo for all their help with paperwork and troubleshooting any issues I had as a graduate student.

I would also like to thank those people outside of Loyola who helped me complete my research. Kevin Duclos, a PhD student at the University of Calgary, has been a tremendous help and resource with my data analysis. He has been very patient teaching me the ins and outs of R coding and I would not have been able to analyze my 3D morphometric data without him.

Finally, I would not have been able to do this thesis without the love and endless support from my family. They have supported me nonstop during my research and my time at Loyola. I cannot thank my mother, Caryn Peters, enough for all her support and help over the years with my research. She was a NICU research coordinator, and she has helped answer plenty of research questions that I have had during my graduate years. She has also been good at annoying me every week to make sure that I finish my thesis in a "timely" fashion. I am forever thankful that my father, Edgar Peters, set me on this path as a child when he would take me fishing every weekend. This is where my passion for fishes and biology all started, so thank you for introducing me to this and providing endless support.

TABLE OF CONTENTS

LIST OF TABLES

LIST OF FIGURES

ABSTRACT

Zeiformes (e.g., Dories, Lookdown dories, Tinselfishes, Oreos) are a deep (1000 m) to mid-water (100 m) marine order of acanthomorph fishes with a circumpolar distribution, and a fossil record extending back to the Late Cretaceous. The order consists of 33 species in six families. The position of the Zeiformes within Teleostei has been debated, but recent studies based on molecular and morphological data place zeiforms within Paracanthopterygii closely related to Gadiformes. Zeiformes are characterized by anal and dorsal profiles that contain a variable number of fin rays and spines. They are mostly deep bodied, highly compressed fishes that exhibit a unique type of jaw protrusibility. This study investigates the jaw morphologies among zeiform families, the variation in jaw protrusion among the taxa, and the evolution of jaw protrusion in the various zeiform lineages compared to previous overall body shape data. Micro CT-scanning technology and three-dimensional geometric morphometrics was employed to observe jaw variation across taxa by using landmarks. Morphospace data showed a similar trend of a star-shaped radiation from an ancestral form like that of Grande et al. (2018), but with differing taxa converging and diverging on each other due to jaw morphologies. This is mostly likely due to modularity of zeiform morphology and developmental constraints, since body form responds to a different set of selective pressures than do the jaws. Furthermore, zeiforms showed considerable variation among taxa with respect to specific bones of the jaw, possibly the result of submodulization and heterochronic shifts in development within the entire craniofacial area.

CHAPTER ONE

INTRODUCTION

Overview of Zeiform Fishes

Zeiformes (e.g., Dories, Lookdown dories, Tinselfishes, Oreos) are a deep to mid-water group of marine acanthomorph fishes with a global circumpolar distribution (Fig. 1), with some species displaying near-worldwide distributions, while others are only regional endemics (such as in the waters off New Zealand and Australia). They are primarily benthopelagic fishes living at depths of 50 to 1000 meters. The zeiform fossil record dates to the Late Cretaceous (late Campanian/early Maastrichtian, 72 mya; Tyler and Santini, 2005; Davesne et al., 2017). The order consists of 33 extant species that are recognized as valid across about six families (Tyler et al., 2003; Tyler and Santini, 2005; Nelson et al., 2016; Grande et al., 2018).

Among the many interesting morphological adaptations of zeiform fishes (e.g., body shape, fin morphology) are that they are known for their highly protrusible jaws and their elongate ascending premaxillary process (Heemstra, 1980; Westneat, 2004; Davesne et al., 2017). This adaptation for increased jaw protrusion has enabled these fishes to effectively capture more elusive prey, such as small crustaceans and small schooling fishes (Bellwood, 2015).

The phylogenetic placement of the Zeiformes within Teleostei has been repeatedly debated. Their history starts with Linnaeus' diagnostic look at the genus *Zeus* in the *Systema Naturae* (Linnaeus 1758). Since then, various zeiform groups have been aligned with different taxa. These included scombrids (Gunther, 1860), chaetodontids and acanthuroids (Starks, 1898),

pleuronectiforms (Holt, 1894; Boulenger, 1902), caproiforms (Regan, 1910), Zeiformes + caproids with beryciforms (Patterson, 1968), within the order Tetraodontiformes (Rosen, 1984), and sister to Beryciformes (i.e., soldierfishes, squirrelfishes, and lanterneyes) + Percomorpha (Johnson and Patterson, 1993), and sister to Tetraodontiformes (Tyler et al., 2003; Tyler and Santini, 2005).

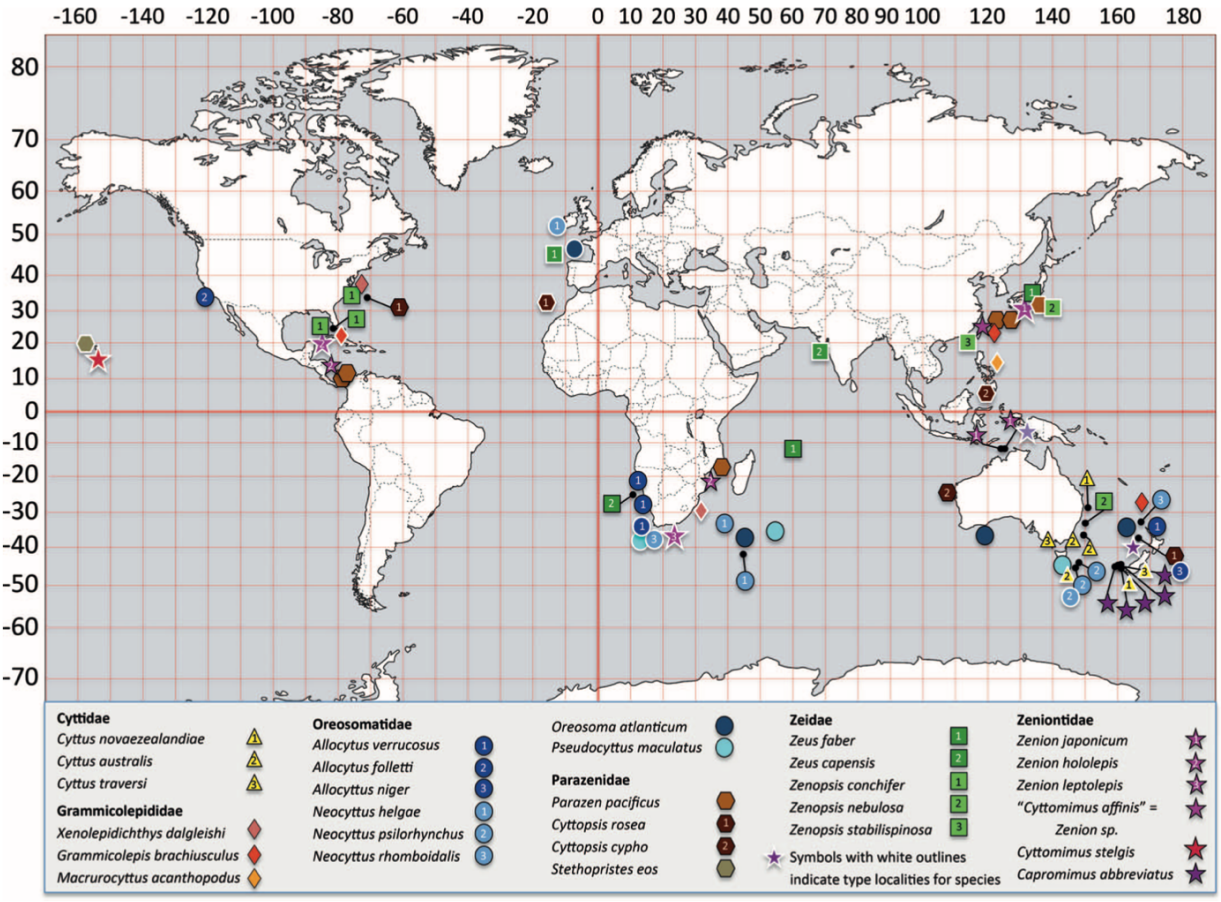

Figure 1. World map showing the collecting localities for specimens from which tissues were obtained for the study of Grande et al. (2018), along with the type locality for each species in the order. Specimen and type localities are most numerous in the western and southwestern Pacific, in the waters surrounding Southern Africa, and on either side of the North Atlantic Ocean (Grande et al., 2018: fig. 1).

Although Tyler et al. (2003: fig. 13) presumed a zeiform + tetradontiform relationship, their work was the first comprehensive phylogenetic study of all zeiform families based on morphological characters. The genus *Cyttus* (family Cyttidae) was concluded to be the sister group to all other extant Zeiformes. Six Zeiform families were recognized, with the following phylogenetic sequence (Fig. 2): Cyttidae (*Cyttus)* — Oreosomatidae (*Pseudocyttus, Allocyttus, Oreosoma, Neocyttus*) — Parazenidae (*Parazen, Cyttopsis, Stethopristes*) — Zeniontidae (*Zenion, Capromimus, Cyttomimus*) — Grammicolepididae (*Macrurocyttus, Xenolepidichthys, Grammicolepis*) — Zeidae (*Zeus, Zenopsis*) (Tyler et al. 2003; Tyler and Santini, 2005).

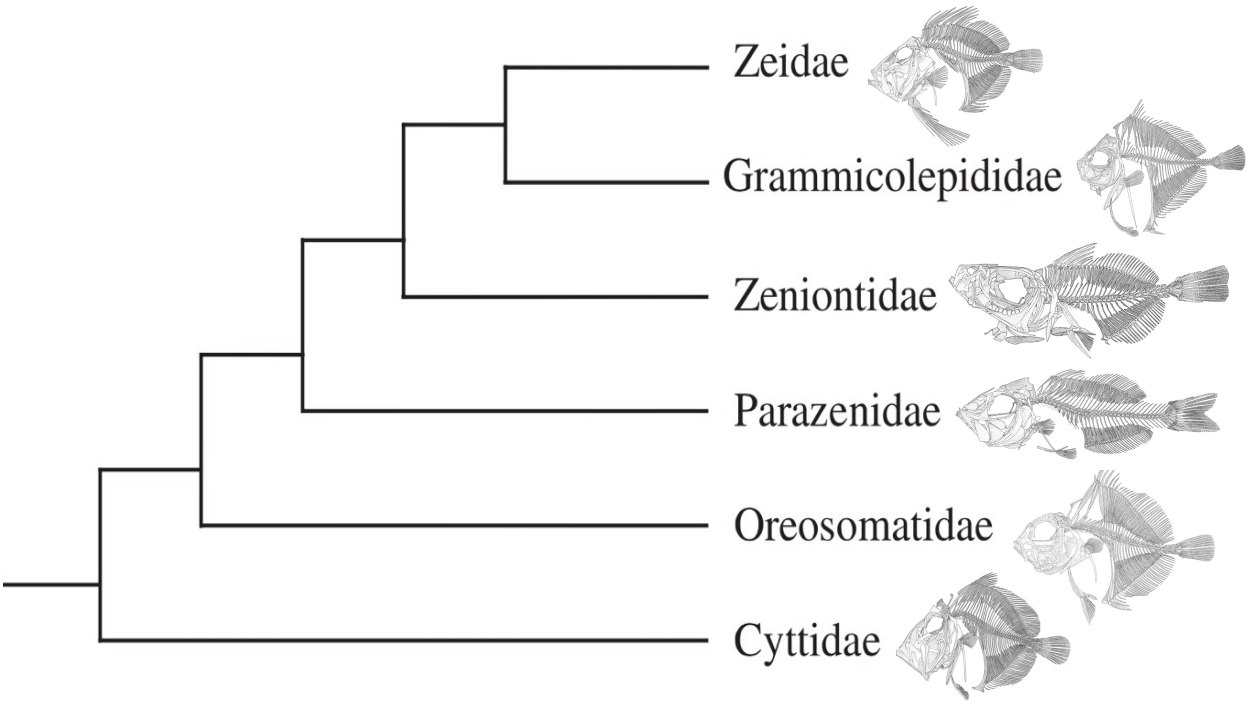

Figure 2. Simplified cladogram showing the interrelationships of the extant zeiform families recovered by Tyler et al. (2003). All line drawings are from Tyler et al. (2003).

The now accepted placement of Zeiformes within Paracanthopterygii was first recognized by Wiley et al. (2000), who placed Zeiformes as sister to Gadiformes (cods). The phylogenetic

placement of Zeiformes within Paracanthopterygii, with the insertion also of *Stylephorus* as sister to Gadiformes by Miya et al. (2007), has been, for more than a decade, supported by both morphological and molecular data (Fig. 3) (e.g., Near et al. 2012; Grande et al., 2013: fig. 1; Borden et al., 2013; Betancur-R et al., 2013; Near et al., 2013; Chen et al., 2014; Davesne et al., 2016; Hughes et al., 2018; Ghezelayagh et al., 2021).

With the new phylogenetic placement of zeiforms within Paracanthopterygii, Grande et al. (2018), using both molecular and morphological characters, once again recovered Zeiformes within Paracanthopterygii and examined the relationships within the order (Fig. 4). In their analysis, *Macrurocyttus* was recovered as basal (sister to the remaining Zeiformes), with Zeidae sister to all others. Among the remaining groups there are two clades. In the first, Parazenidae are sister to Grammicolepidae and Zeniontidae. In the second, Cyttidae are sister to (*Capromimus* + *Cyttomimus*) plus Oreosomatidae (Grande et al., 2018).

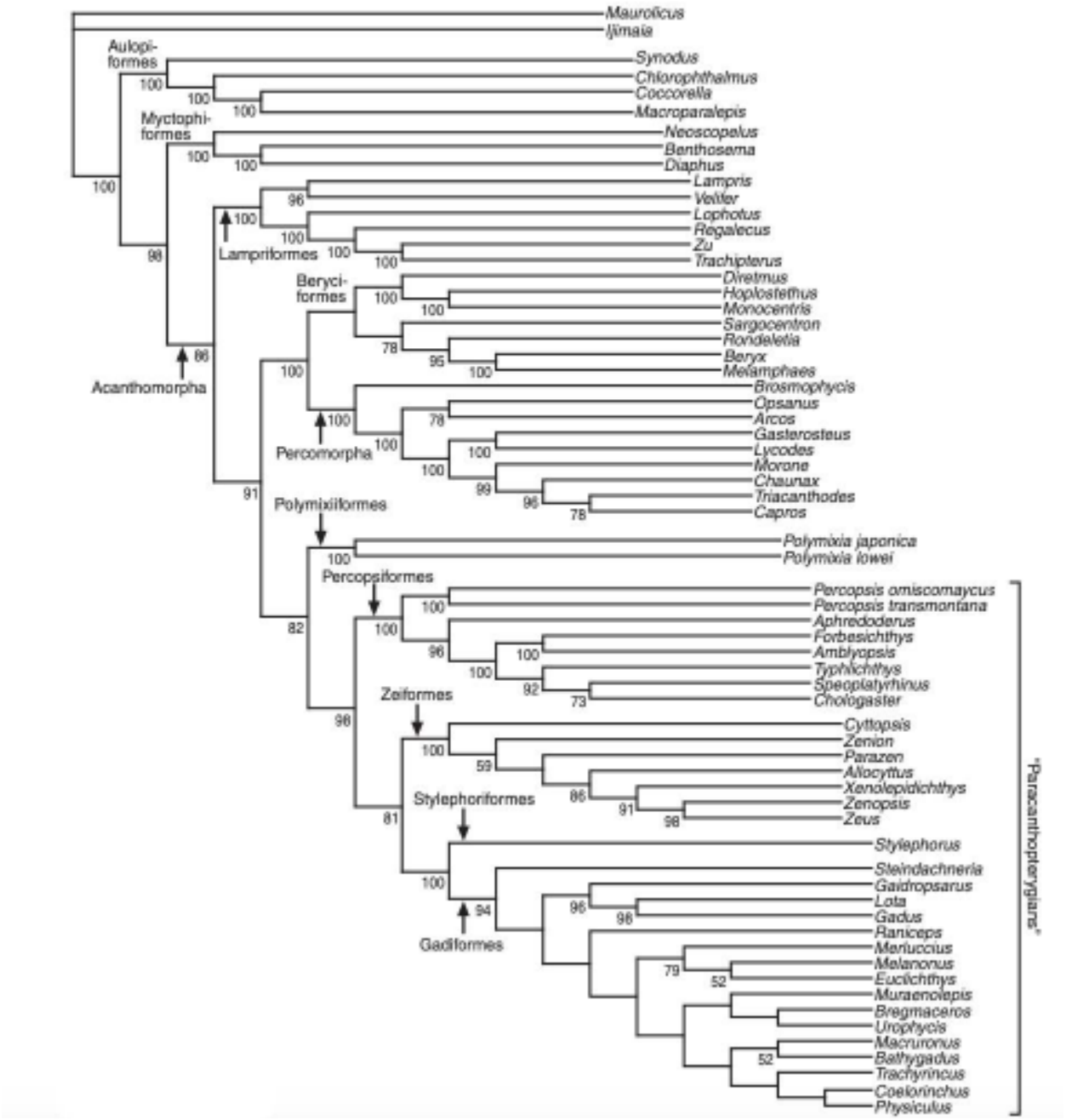

Figure 3. Supported phylogenetic placement of Zeiformes within Paracanthopterygii, with a sister relationship to Gadiformes + Stylephoriformes (from Grande et al. 2013). The paracanthopterygian clade contains [Percopsiformes + ((Gadiformes + *Stylephorus*) + Zeiformes] and in more recent work it also includes the Polymixiiformes.

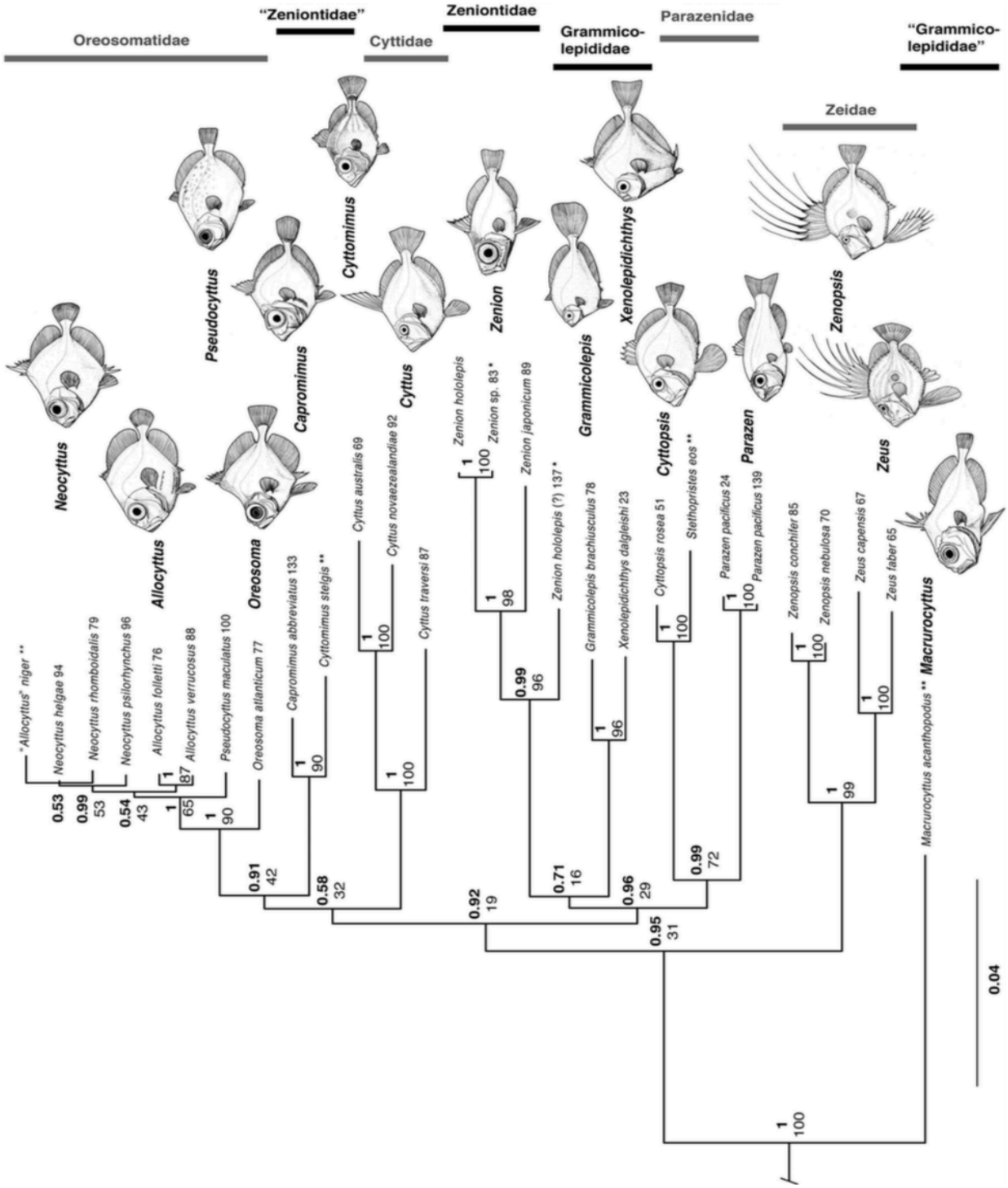

Figure 4. Combined (total-evidence) molecular and morphological phylogeny of the Zeiformes based on Bayesian inference (BI) using MrBayes v.3.1.2 from Grande et al. (2018).

Geometric Morphometrics

Geometric morphometrics have recently been established as efficient tools to quantify differences in overall body shape or specific morphological structures to be applied to evolutionary biology. This allows scientists to deal with geometric landmarks that produce 2D or 3D coordinate data that can be further analyzed. Traditionally, scientists would use character-based morphometrics or univariate measurements to make inferences about phylogenetic relationships. These new analyses are often important because they can allow scientists to support previous conclusions based on earlier methods, or in some cases it may generate new insights or evolutionary trends. For example, geometric morphometrics has detected additional differences in beak size and shape of Darwin's finches and allowed for better discrimination among species. Furthermore, these results have generated new hypotheses, ecological trends, and diversification patterns (Foster, 2008).

General Zeiform Morphology

Based on Grande et al. (2018), the fishes of order Zeiformes are arranged within the following clades (Figure 5): *Macrurocyttus* (formerly in Grammicolepididae), Zeidae (*Zeus* + *Zenopsis*), Parazenidae (*Parazen* + [*Cyttopsis* + *Stethopristes*]), Grammicolepididae (*Grammicolepis* + *Xenolepidichthys*), Zeniontidae (*Zenion*), Cyttidae (*Cyttus*), (Cyttomimus + Capromimus, both formerly in Zeniontidae), and Oreosomatidae (*Oreosoma*, *Pseudocyttus*, *Allocyttus*, and *Neocyttus*).

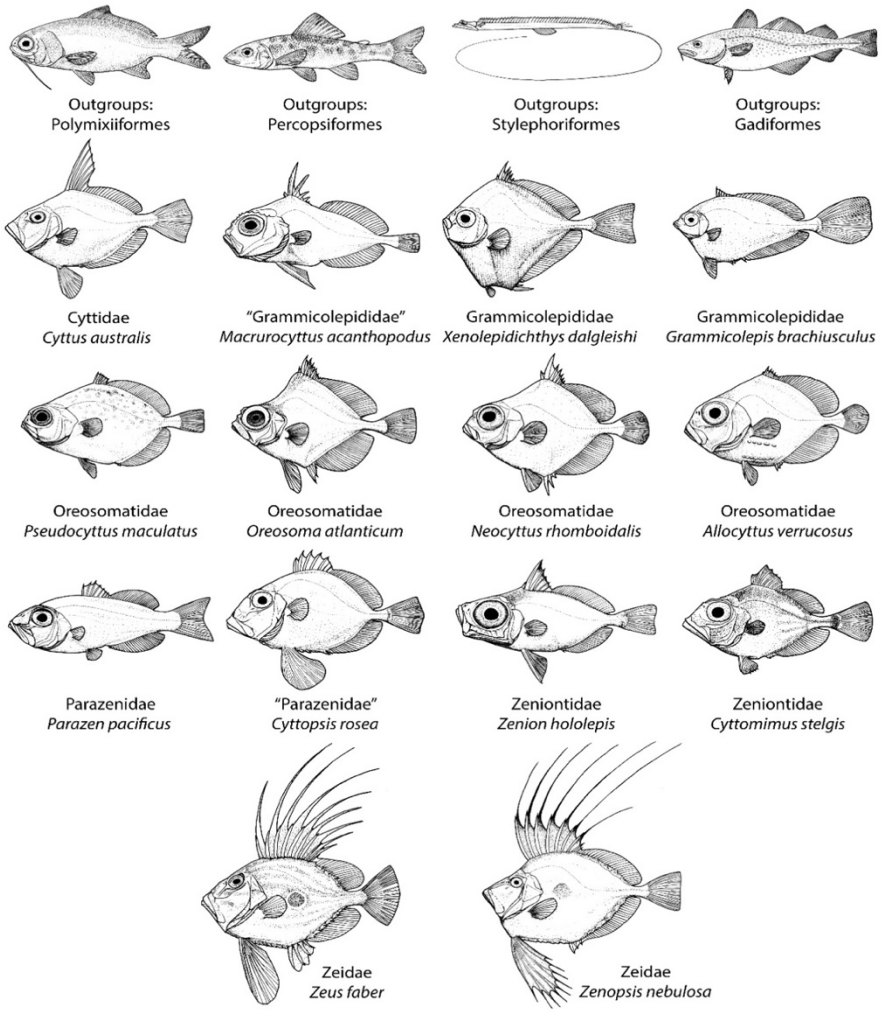

Figure 5. Zeiform taxa illustrating representative body forms, along with selected outgroup taxa, from Grande et al. (2018). Illustrations drawn by Michael Hanson.

Zeiformes are characterized by anal and dorsal profiles that contain a variable number of fin rays and spines. They are mostly deep bodied, highly compressed fishes that exhibit a unique type of protrusible jaws (Fig. 6) with elongated premaxillary ascending processes that reach past the front of the orbital bones (the ascending process is medial to the orbital bones), and articular processes (Tyler et al., 2003). Cyttidae (Lookdown or Big-eye dories) are large-bodied fishes

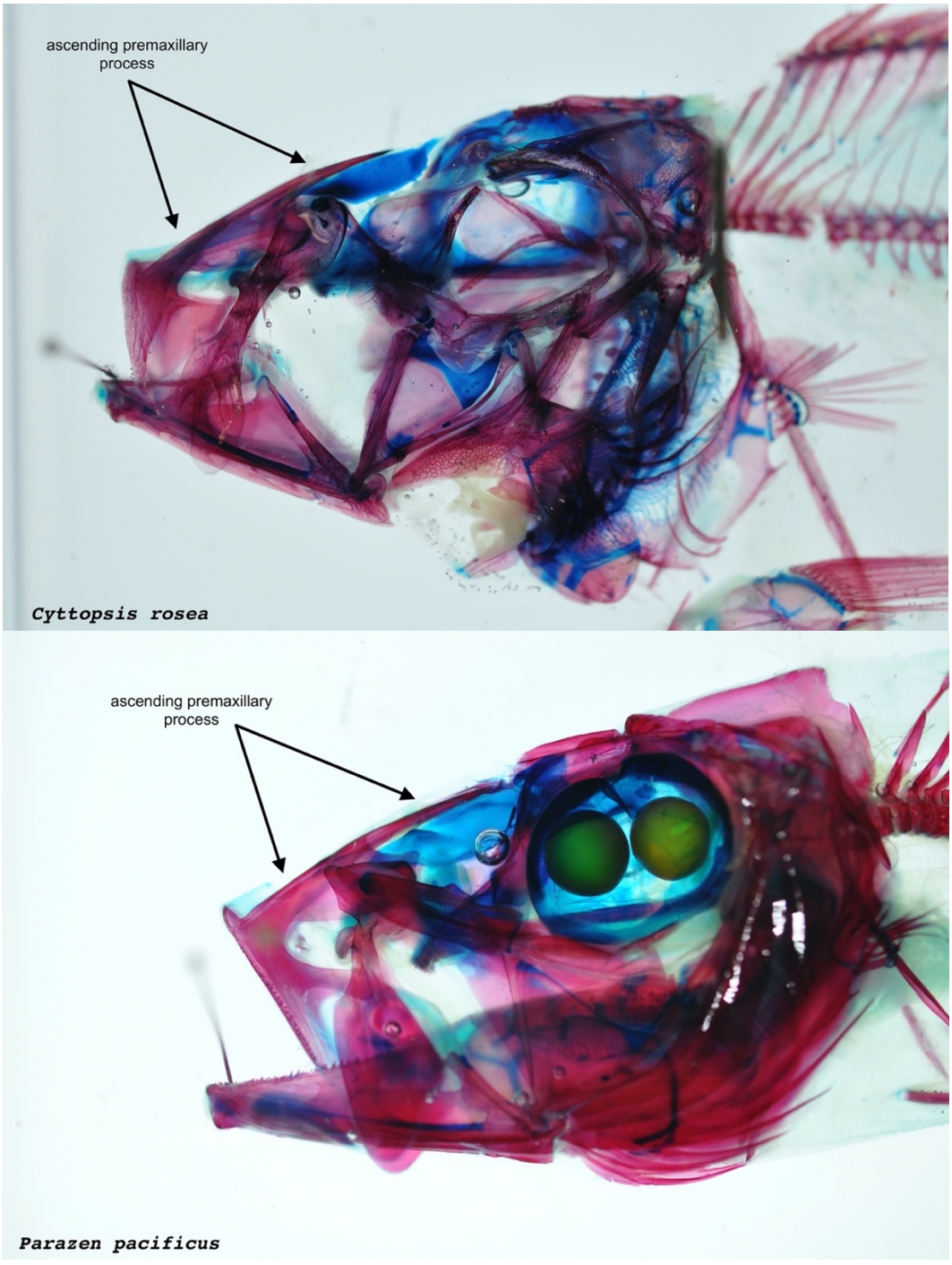

Figure 6. Cleared and stained specimens of *Cyttopsis rosea* (Top: FMNH 67091) and *Parazen pacificus* (bottom: FMNH 67158) with mouth open to show jaw protrusion. The ascending process of the premaxilla is labeled to show how it slides anteriorly to increase the level of upper jaw protrusion.

with large mouths and a long ascending premaxillary process (reaching behind the front border of the orbit, about one-half into orbit), found through the southeast Atlantic and Indo-Pacific oceans. Oreosomatidae (Oreos) have an extended juvenile stage and display moderate to large mouths with a moderate ascending process (reaching from front border of orbit to behind front border and one-fifth into orbit), found throughout the Southern Hemisphere. Parazenidae (Slender or smooth dories) exhibit a more elongate body form than most other zeiform genera, large and oblique jaws with a moderate ascending process (reaching behind front border of orbit one-fifth to one-third into orbit) and are found across the Atlantic and Pacific oceans. Former zeniontids (Armor-eye and Capro dories) exhibit moderately deep to slender body forms with moderate mouths and a moderate ascending process (reaching behind front border of orbit about one-fifth to one-third into orbit), found primarily in waters off the southern coast of Africa and in the western Pacific. Grammicolepidae (Dwarf dories) display smaller to moderate jaw sizes relative to their body with moderate ascending process (reaching from front border of orbit to behind front border about one-fifth into orbit): they are found throughout the Atlantic and Pacific oceans. Zeidae (Buckler or John dories, St. Peter's fish) are more popularly known members of the order as they are prepared and sold as restaurant dishes; they exhibit larger mouths with moderate ascending processes (reaching to about the front of the orbit), and are found in the Atlantic, Pacific, and Indian oceans (Tyler et al., 2003).

This group of fishes exhibits variation in the amount of jaw protrusion, with *Parazen* and *Zenion* showing relatively longer and more oblique jaws compared to Oreosomatidae, Cyttidae, and *Cyttopsis*, which have shorter, less oblique jaws. Highly protrusible jaws have been an important innovation in the feeding mechanism of teleostean fishes in the last 200 million years.

Protrusibility enables them to capture smaller and more elusive prey and could be an important factor in their evolutionary success (Staab et al., 2012; Bellwood, 2015). Zeiform jaw protrusion and mechanics are unique from those of other paracanthopterygians such as *Polymixia* (Fig. 7) and other acanthomorphs in general.

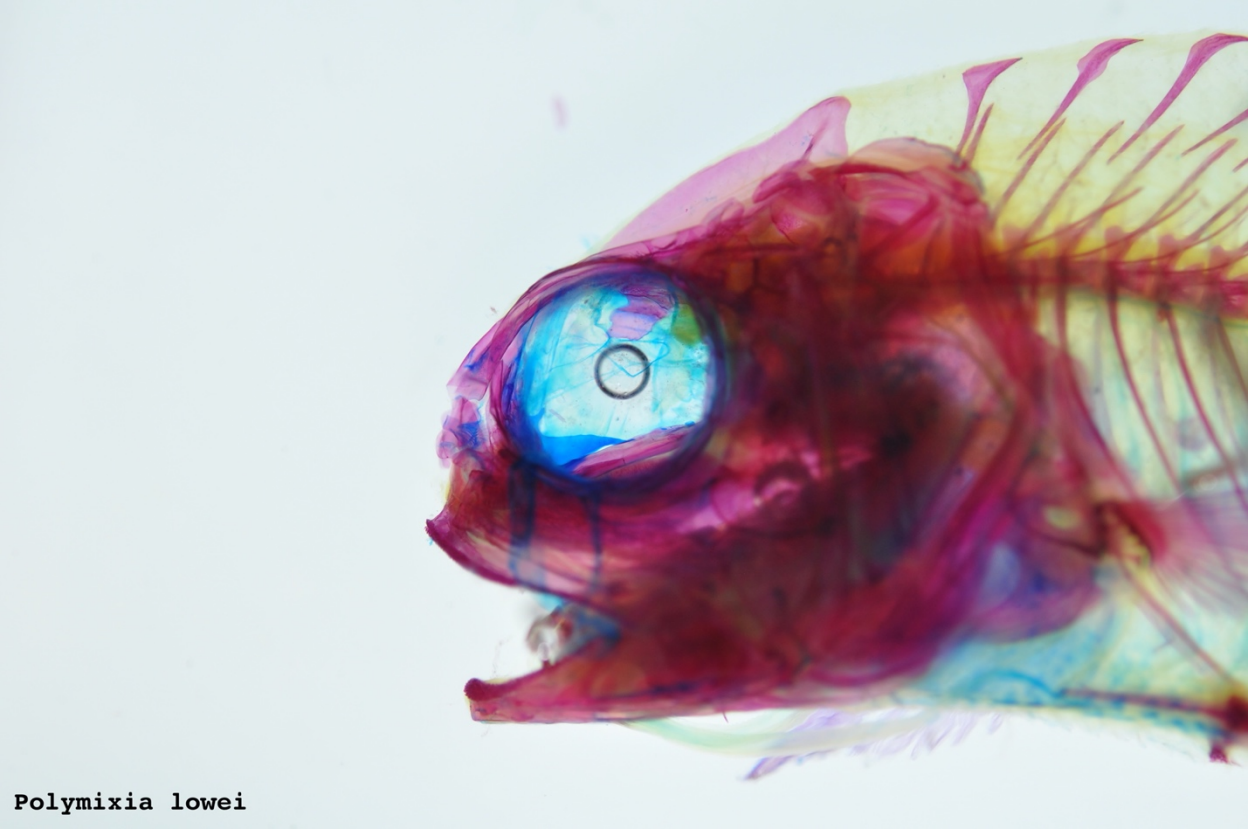

Figure 7. Cleared and stained specimen of *Polymixia lowei* (UF 127145) with mouth open to show the limited jaw protrusion of a paracanthopterygian that is closely related to Zeiformes.

Westneat et al. (2004) shows the importance of upper jaw protrusion due to a four-bar linkage mechanism (Fig. 8) that initially arose in Zeiformes and has evolved multiple other times in ray finned fishes (Actinopterygii). This mechanism is due to a rotational palatine linkage with

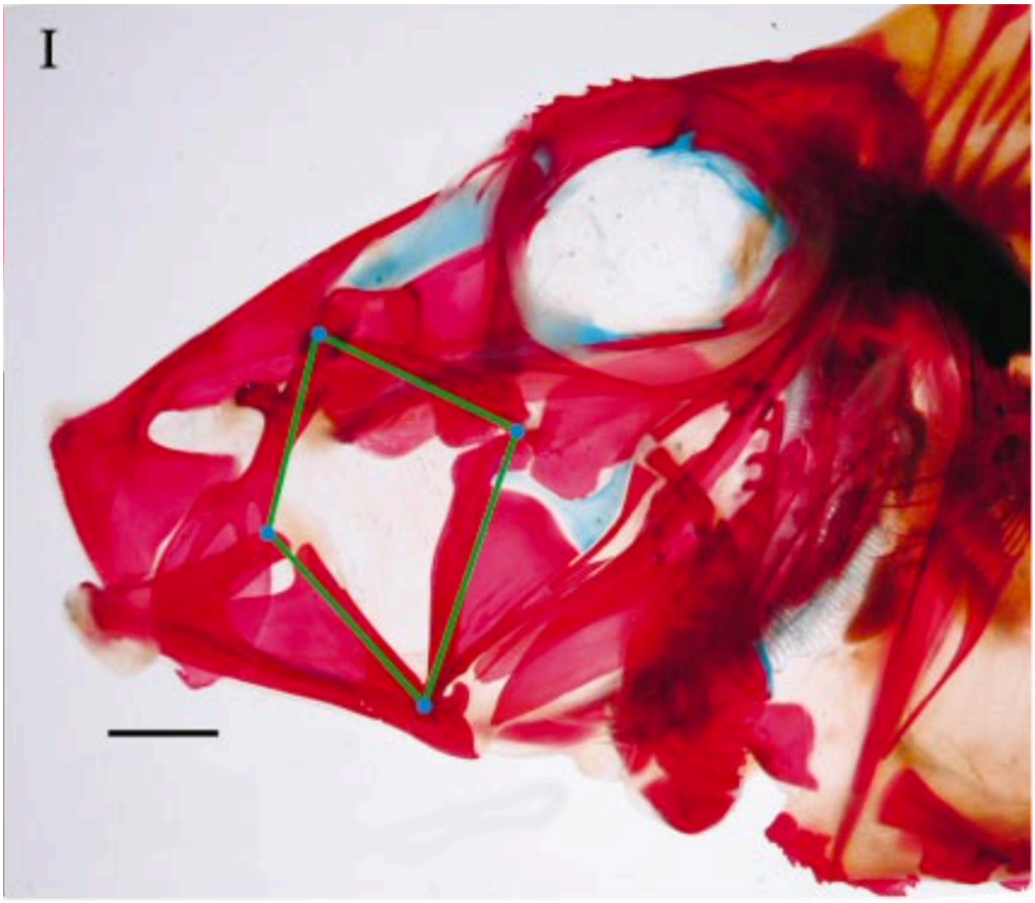

Figure 8. The earliest clade to show an anterior jaw four-bar linkage with a rotational palatine that powers protrusion is the dories illustrated by the rosy dory, *Cyttopsis rosea.* Scale bar = 5 mm. Modified from Westneat (2004).

the suspensorium (fixed link), a freely rotational maxilla, and the ascending process of the premaxilla able to slide anteriorly to increase the level of jaw protrusion and mouth gape (Westneat, 2004). The hypothesized fulcrum of lower jaws in teleost fish is the angular articular joint, which is included as one of the landmarks due to its importance in teleost fish feeding and musculoskeletal functions. The alveolar process of the premaxilla (lowest area of the premaxillary extension) and post maxillary process, which is the lower of the two ventral premaxillary flanges, attaches to the upper jaw. These two premaxillary processes are very

important in biting/feeding mechanics for all zeiforms. The upper of these two flanges is what creates one of the four linkages in the four-bar jaw linkage seen in all extant Zeiformes (Westneat, 2004). The suspensorium plays a role in this four-bar linkage mechanism for feeding by connecting the lower jaw (quadrate bone and symplectic bone) with the base of the skull near the hyomandibular bone. The input linkage for these fish is the lower jaw, which includes the articular and dentary. All these bones are included in my list of landmarks to help capture the variation in jaw protrusion and feeding of Zeiformes (See Chapter 2: Materials & Methods).

Purpose

It has been hypothesized that zeiform evolution is an example of an adaptive radiation, as is suggested by its rapid radiation and the short branches seen in its phylogeny (Fig. 4). My research will test this hypothesis by examining a discrete and novel character set (i.e., jaw morphology) across the zeiform families with a focus on genus- and family-level relationships. This will allow us to further understand the evolution and relationships of Zeiformes. Furthermore, understanding zeiform jaw disparity and how their jaws work could help us to eventually understand and infer the foraging behaviors and diet of these elusive fishes.

Objectives

(1) Morphometric studies of zeiform fishes to date have focused on overall body shape and fin variation (Grande et al., 2018). My research will add information about the variation seen in jaw morphology across all families and test the phylogenetic relationships of Grande et al. (2018).
(2) I will analyze the mechanics of jaw protrusion in representative Zeiformes. Furthermore, I will examine variation in jaw protrusion and test whether it is linked to differences in diets, habitat depth, and geographic distribution. By examining phylogenetic changes in jaw protrusion

across Zeiformes, I will be able to reconstruct the ancestral states at various points in the phylogeny. I plan to investigate this using a phylomorphospace analysis of jaw morphologies, as conducted for body shape by Grande et al. (2018). This will help us to see any patterns of convergences and divergences amongst the taxa of this group. By investigating the evolution of jaw protrusion in Zeiformes, we may be able to understand their rapid radiation and evolutionary success.

CHAPTER TWO

GEOMETRIC MORPHOMETRICS OF THE ORDER ZEIFORMES USING 3D MICRO-CT SCANNER

Over the last 50 years, the field of morphometrics and shape analysis has undergone revolutionary changes with the introduction of geometric morphometrics (Adams et al., 2004) (Rolf and Marcus 1993). Traditionally, morphometric analyses were conducted using linear measurements such as length, height, and width, or by creating character matrices describing differing morphological traits varying across taxa. The new landmark-based approach of geometric morphometrics allows scientists to retain more information of the original organism's shape after multivariate analyses (Adams et al., 2004). Geometric morphometrics started using landmarks via a 2D framework, allowing for more in-depth morphological analyses to look at evolution across taxa and more accurately observe their interrelationships (Foster 2008). Now with access to 3D technology, more research is being conducted using radiographs and micro-CT scanners. For this study, micro-CT scanning was used to explore a novel character set within an order Zeiformes.

With developments in the field of statistics there also came a higher degree of sophistication in shape analysis. This led to multivariate morphometrics where measurements could be further analyzed using principal component analysis, multivariate regression, partial least squares, modularity tests, and related methods (Adams et al., 2004). New geometric

morphometrics tools offer a wide range of methods for shape change analysis and visualization in different biological contexts (Klingenberg and Lobon 2013).

Materials and Methods

Three dimensional morphometrics analyses were conducted to analyze and compare the variation in zeiform jaw shapes. All adult specimens for this study had intact jaws and were scanned using a Perkin Elmer Quantum GX2 micro-CT scanner. Specimens for this study were borrowed from museum collections (See Materials Examined). Eleven of the 16 zeiform genera were represented in the data set. The rarity of some zeiforms in museum collections prohibited their inclusion in this study (i.e., Exceptions were *Neocyttus, Pseudocyttus, Cyttomimus, Grammicolepis,* and *Macrurocyttus)*. Of the included taxa, depending on availability, one to five specimens per genus were examined for this study (see Materials Examined). All specimens were large alcohol-preserved juveniles or adults, ranging from 45–157mm SL, with closed jaws.

Materials Examined

All specimens examined in this study for landmarking and micro-CT scanning were alcohol specimens (Alcohol) preserved in 75% ethanol.

Institutional abbreviations: FMNH, Field Museum of Natural History; KU, University of Kansas Museum of Natural History; LACM, Natural History Museum of Los Angeles County; MCZ, Museum of Comparative Zoology; USNM, Smithsonian National Museum of Natural History.

Parazenidae. ---*Parazen pacificus:* 5 specimens, 95.2-100.2mm SL: FMNH 65401, FMNH 64402, FMNH 64403, USNM 364277(Alcohol), FMNH 67158 (CS).

Cyttopsis rosea: 6 specimens, 62.2-143.8mm SL: FMNH 67093, FMNH 67095, FMNH 67097, USNM 377980 (Alcohol), FMNH 67091 (CS).

Zeidae. ---*Zenopsis conchifer:* 13 specimens, 42.3-105.4mm SL: FMNH 67090, USNM 159819, USNM 372241 (Alcohol), FMNH 67179 (CS).

Zeus faber: 4 specimens, 76.00-113.00mm SL: USNM 325986, FMNH 4062 (Alcohol), USNM 307842 (CS).

Zeniontidae. ---*Zenion hololepis:* 4 specimens, 60.3-84.4mm SL: USNM 377986, FMNH 64410.

Capromimus abbreviatus: 5 specimens, 70.8-80.4mm SL: TAN 1308.

Grammicolepidae. ---*Xenolepidichthys dalgleishi:* 4 specimens, 55-78.2mm SL: FMNH 74320.

Cyttidae. ---*Stethopristes eos:* 1 specimen, 105.2mm SL: USNM 226570.

Cyttus australis: 1 specimen, 167.9mm SL: MCZ 17264.

Oreosomatidae. ---*Oreosoma atlanticum:* 1 specimen, 127.6mm SL: KU 33415.

Allocyttus verrucosus: 1 specimen, 142.2mm SL: LACM 44752.

Micro-CT Scanning

Thirty-seven micro-CT scans of the tip of the snout to the first few vertebrae were taken to represent all extant zeiform families. All specimens were scanned in a Perkins-Elmer Quantum GX2 Micro-CT Imaging System provided by Loyola University's Biology Department. Due to the size of the scanner's chamber, each specimen was scanned one at a time in the same orientation. They were placed flat in Ziploc® bags to preserve the specimens and not allow them to dry out during scanning. High resolution 14-minute scans were taken using a standard Copper Aluminum filter (Cu 0.06 + Al 0.05) for obtaining the best bone clarity. Some smaller specimens were scanned for 57-minutes to obtain the highest micron resolution. Because

of the low bone density of the smaller specimens, the 14-minute timed scan was not adequate to see enough bone clarity for landmarking. Scans of the anterior portion of the body were then exported as slices using a DICOM formatted file for further data analyses.

Landmarking

DICOM stacked files were loaded into Stratovan Checkpoint 3D landmark editor software (Version 2018.08.07). Once loaded, scans were visualized by creating an isosurfaced volumetric scan of the specimen by extracting a surface from 3D volumetric data and adjusting the density gradient to the desired volume. All landmarks were then digitized accordingly, and coordinate data was exported as centimeters in Morphologika format.

Twenty-three homologous landmarks (Table 1) were chosen to capture variation involved in the feeding and jaw mechanics of these fishes. Of the twenty-three landmarks, six were located internally, while the other seventeen were located externally and can be seen in a 2D photo of the specimen (Fig. 9). To aid in landmarking accurately, I used volume rendered 3D models of each specimen from 3D slicer 4.10.2 (Fedorov et al., 2013) to visualize each bone in better detail (Fig. 9). Tyler et al. (2003) was used for detailed descriptions of zeiform jaw anatomy. Lateral skeletal drawings from Tyler et al. (2003) were used for visual learning and to help with side-by-side bone recognition during landmarking in Stratovan (Fig. 10). Due to the nature of the bone density slider in Stratovan, it was difficult to be able to visualize some bones that were less dense. Stratovan allows users to establish multiple density volumes to help with landmarking internal bones that are being hidden by larger more dense areas.

Landmark #	Landmark Description
1	Anterior tip of premaxilla
2	Ventral tip of premaxilla
3	Dorsal tip of premaxilla
4	Posterior extent of ventral flange (premaxilla)
5	Posterior extent of dorsal flange (premaxilla)
6	Anterior-dorsal tip of maxilla
7	Anterior-ventral tip of maxilla
8	Posterior tip of maxilla
9	Anterior-dorsal tip of dentary
10	Anterior-ventral tip of dentary
11	Posterior-dorsal tip of dentary
12	Posterior-ventral tip of dentary
13	Posterior extent of articular
14	Dorsal tip of articular
15	Base of angulo-articular joint
16	Posterior extent of retroarticular
17	Ventral tip of preopercle
18	Dorsal tip of preopercle
19	Ventral extent of symplectic
20	Dorsal extent of symplectic
21	Ventral tip of hyomandibula
22	Dorsal anterior extent of hyomandibula
23	Dorsal posterior extent of hyomandibula

Table 1. List of all twenty-three landmarks and their location descriptions.

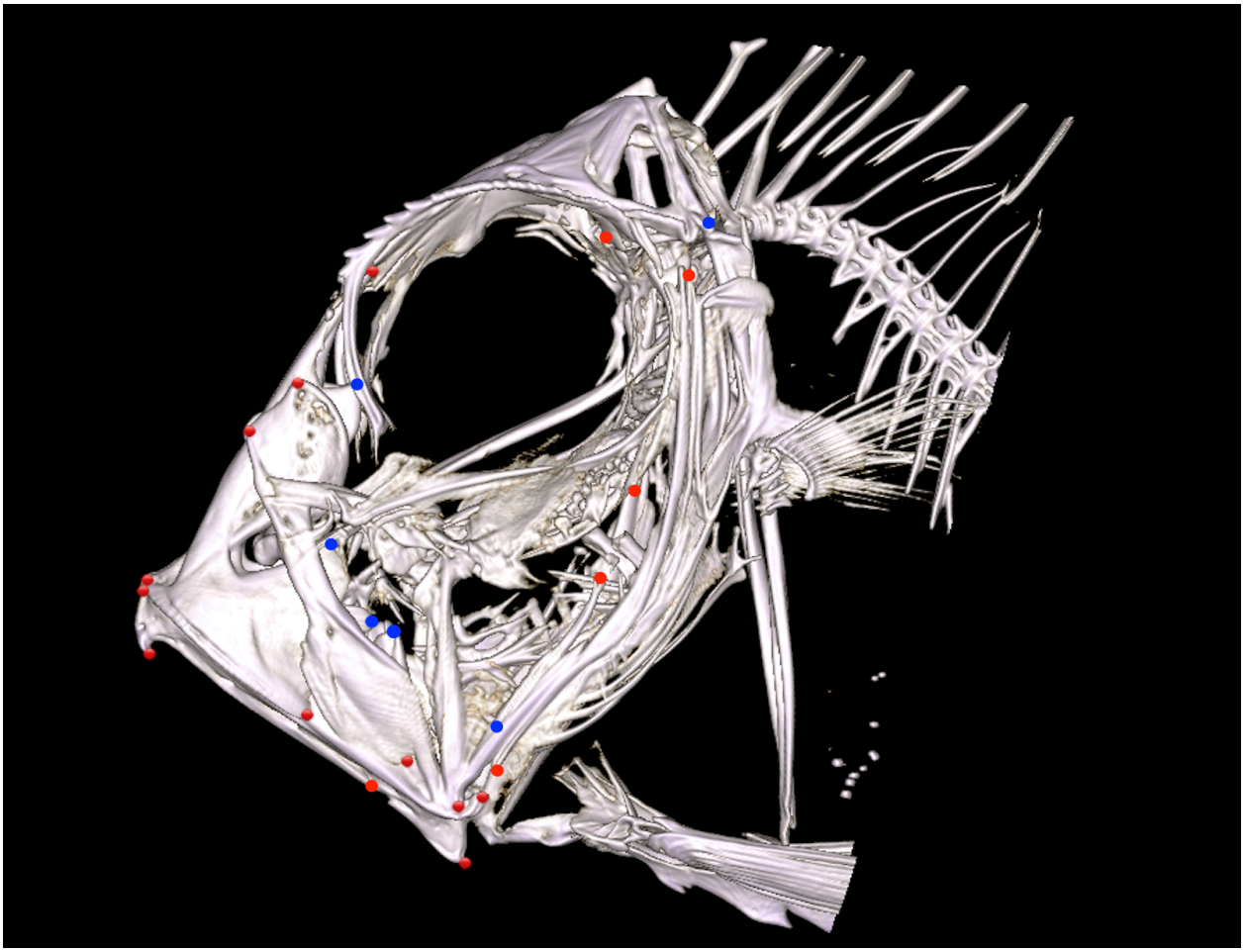

Figure 9. An isosurface micro-CT scan of *Cyttopsis rosea* (FMNH 67093) showing all twenty-three internal (blue) and external (red) landmarks.

As mentioned by Tyler et al. (2003), Zeiformes display great premaxillary variation, with varying lengths of elongation on the ascending process. The increasing length of this process is indicative of a greater degree of protrusibility. Most zeiforms have ascending processes that are so long that they reach back past the orbital bones (Tyler et al., 2003). The ascending premaxillary process seems to stop at the orbital bones for the families *Oreosomatidae* and *Zeidae*. All other families display an ascending premaxillary process that reaches only slightly

past the orbital bones. In addition to looking at the overall jaw variation seen across zeiforms, a smaller scale comparison of just the premaxilla shape variation for all specimens was included.

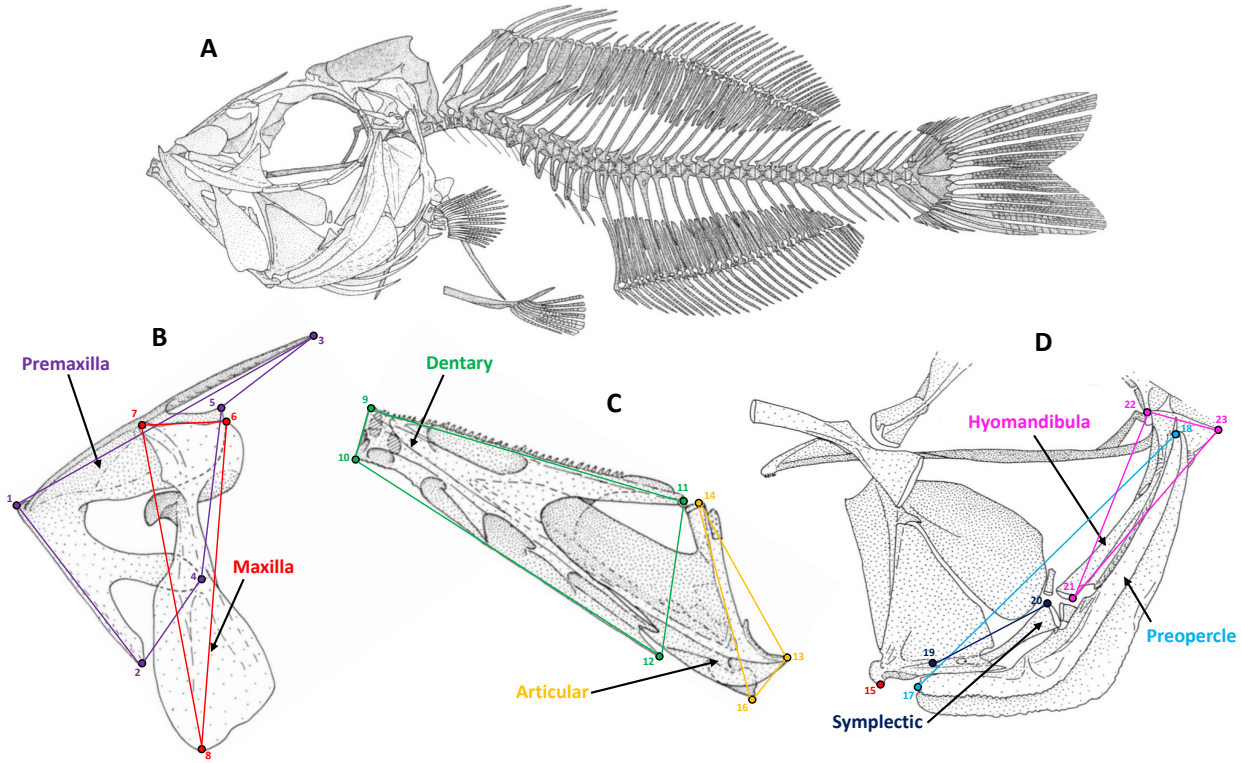

Figure 10. Line drawing of the skeleton of *Parazen pacificus* from Tyler et al. (2003), showing upper jaw bones, lower jaw bones, and bones of the suspensorium. (A) Parazenidae. *Parazen pacificus*, CAS 38404, 96mm SL, lateral view. (B) Landmarks 1-8 of the upper jaw, which include the premaxilla and maxilla bones. (C) Landmarks 9-16 of the lower jaw, which include the dentary and articular bones. (D) Landmarks 17-23 of the preopercle bone and suspensorium, which includes the symplectic and hyomandibula. All line drawing images were taken from Tyler et al. (2003). For specific landmarks refer to Table 1 above.

Data Analysis

All data analyses were performed using the 'Geomorph' (v4.0) package in R using RStudio (v1.4.1717). All landmark coordinated were loaded into R Studio in Morphologika formatting. Landmarks were all plotted unilaterally, except for specimen thirteen in which we had to flip the x-axis so that all coordinates were aligned in the proper planes. They were then

extracted as a list so that we could then perform a procrustes superimposition on all coordinates. A traditional Principal Components Analysis based on OLS-centering and data projection was performed using the updated R function `prcomp`.

Landmarks were subjected to Procrustes fit aligned by principal axes, and then a covariance matrix was generated from these coordinates. Procrustes coordinates were then subjected to principal component analysis (PCA). All species were classified by family following the most recent phylogenetic relationships from Grande et al. (2018). The shape changes corresponding to the first three principal components of the PCA were then analyzed using 3D wireframe diagrams (Fig. 11). Wireframe diagrams displaying shape changes among specific bones were shown for the first two principal components. These bones included the premaxilla, maxilla, dentary, articular, symplectic, preopercle, and hyomandibula. Each individual bone had associated wireframe diagrams displaying the maximum and minimum measurements for principal components one and two. These allowed for better visual analyses of variation that was seen in each landmarked bone.

The combined evidence phylogeny, from Grande et al. (2018), was mapped into the PCA morphospace to create a phylomorphospace. This was done in R using a phylogenetically aligned PCA analysis, in which the phylogeny is considered during the analytical step of ordination. In the phylomorphospace, the rapid radiation of the phylogeny near the root of the tree is observed. This analysis was conducted using code in R from Revell et al. (2009) and Polly et al. (2013). Average species shapes from all 27 landmarks were plotted against the Bayesian inference combined evidence (morphological and molecular) phylogeny from Grande et al. (2018).

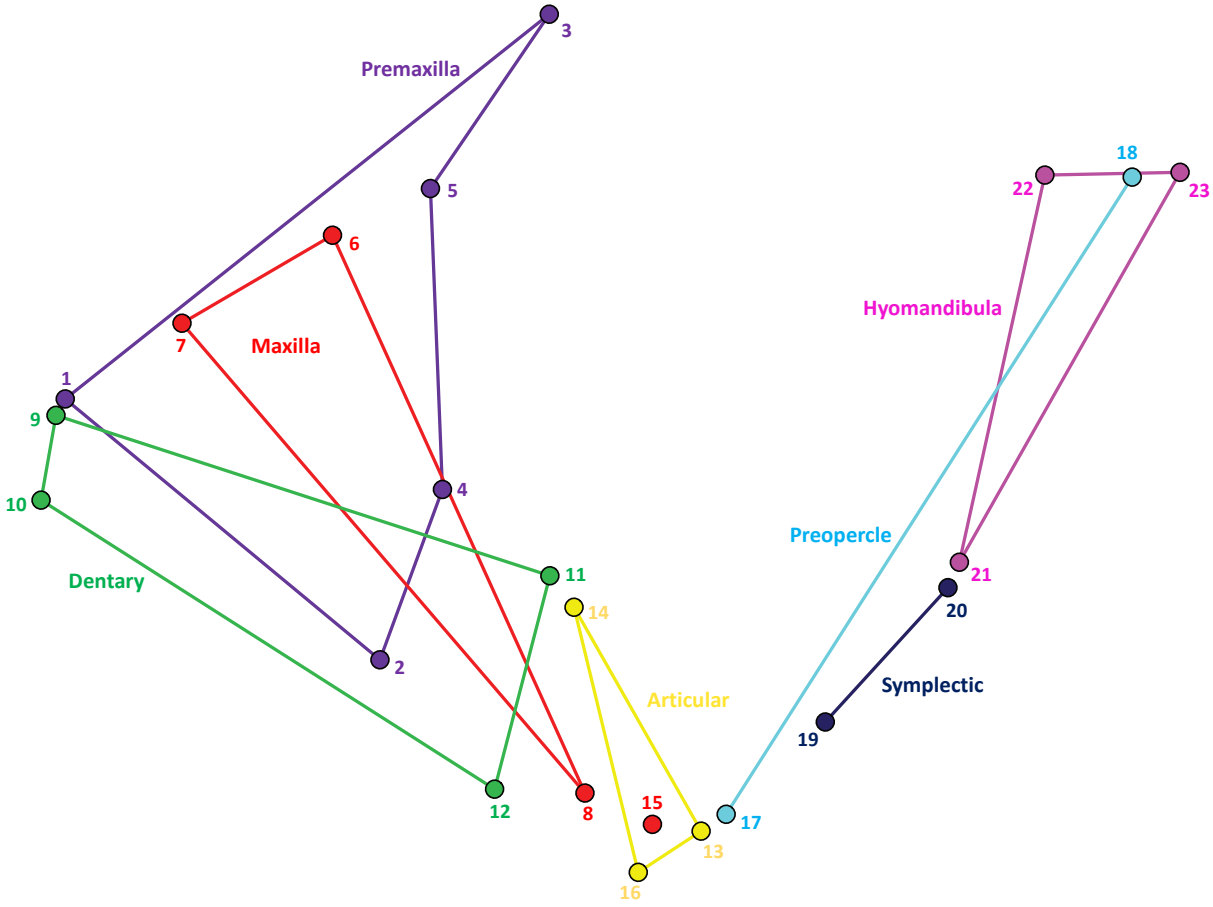

Figure 11. 2D wireframe diagram of all 23 landmarks for *Parazen pacificus*. Each bone from Figure 10 is included here, with matching color coding and landmarks. This is used as a template for reading 2D wireframe diagrams in the results section (Figs. 13, 14, and 16). For specific landmark descriptions refer to Table 1.

CHAPTER THREE

RESULTS

All data analyses were performed using the 'Geomorph' (v4.0), ggplot2, morpho, ape, and abind packages in R (Adams et al., 2022; Baken et al., 2021).

OBJECTIVE ONE

Principal Components Analysis

Principal components analysis (PCA) of Procrustes coordinates from 23 landmarks (Table 1) of 11 zeiform species produced principal components, of which the first three explain more than 73% of the total variance (PC1 29.7%, PC2 22.9%, and PC3 21.6%). Although it is unusual, the total variances explained by the first 3 principal components are nearly equal, meaning they are nearly equally important for summarizing jaw disparity. The plot of PC 1 vs. 2 shows strong species grouping without any outliers (Fig. 12). *Parazen pacificus* shows the maximum variation in the negative direction of PC1, whereas *Zenopsis conchifer* shows the maximum variation in the positive direction of PC1. The wireframe for PC1 (Fig. 13) illustrates that the first component corresponds to differences in overall jaw length and height, with a shift from the minimum PC1 capturing longer and vertically shorter jaws to maximum PC1 portraying a vertically longer and shorter jaw shape. Furthermore, PC1 captures a change in the relative size and length of the premaxillary bones, with an increased premaxillary ascending process at the minimum of PC1 versus the maximum. *Cyttopsis rosea* falls near the center of both principal components 1 and 2, displaying a near average jaw shape for both components.

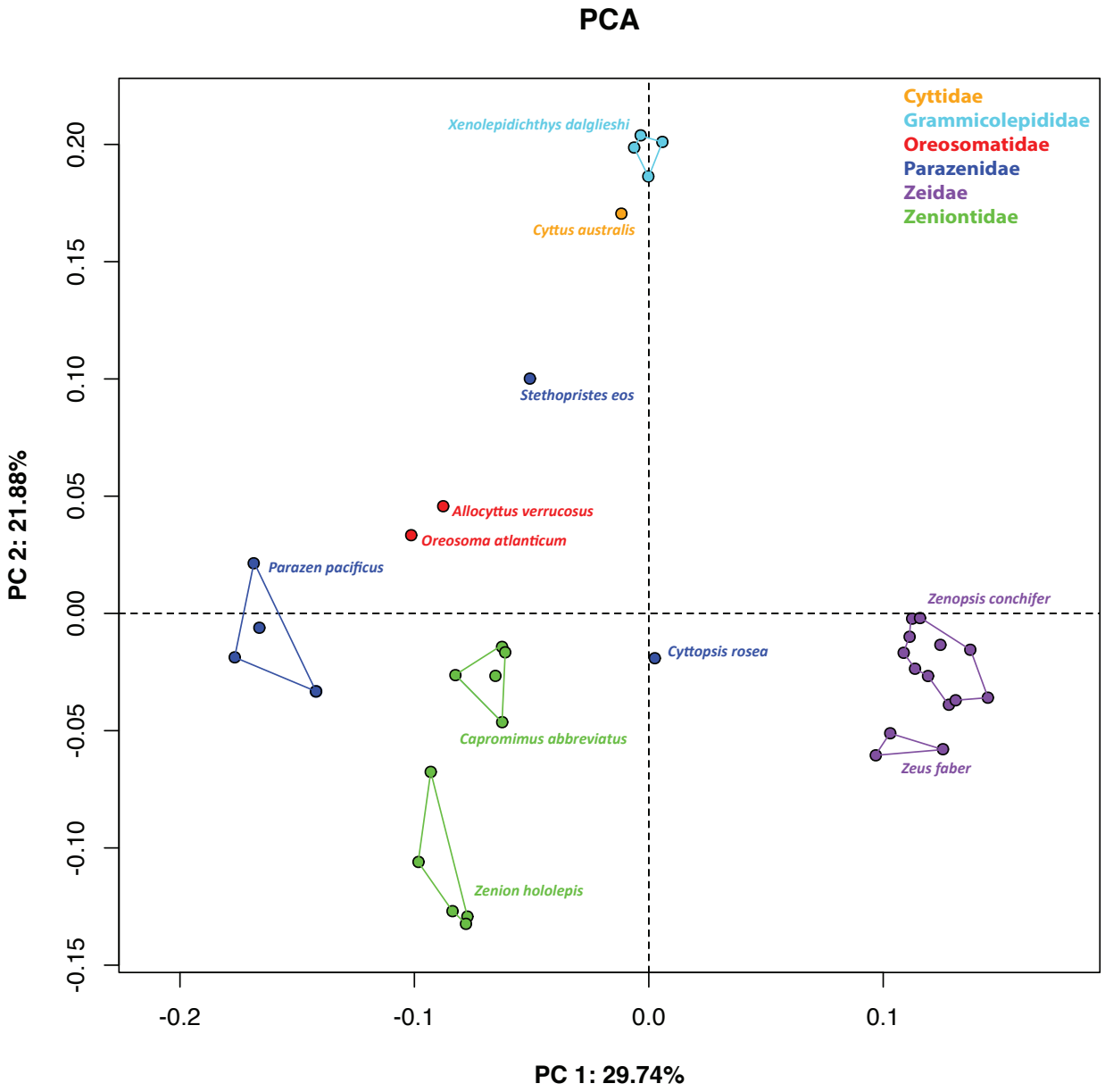

Figure 12. Principal Components Analysis plot of all 23 landmarks done on 36 Zeiform specimens. The x-axis shows Principal Component 1 (PC1), whereas the y-axis displays Principal Component 2 (PC2). Each represented Zeiform family as originally recognized by Tyler et al. (2003) is specified by color.

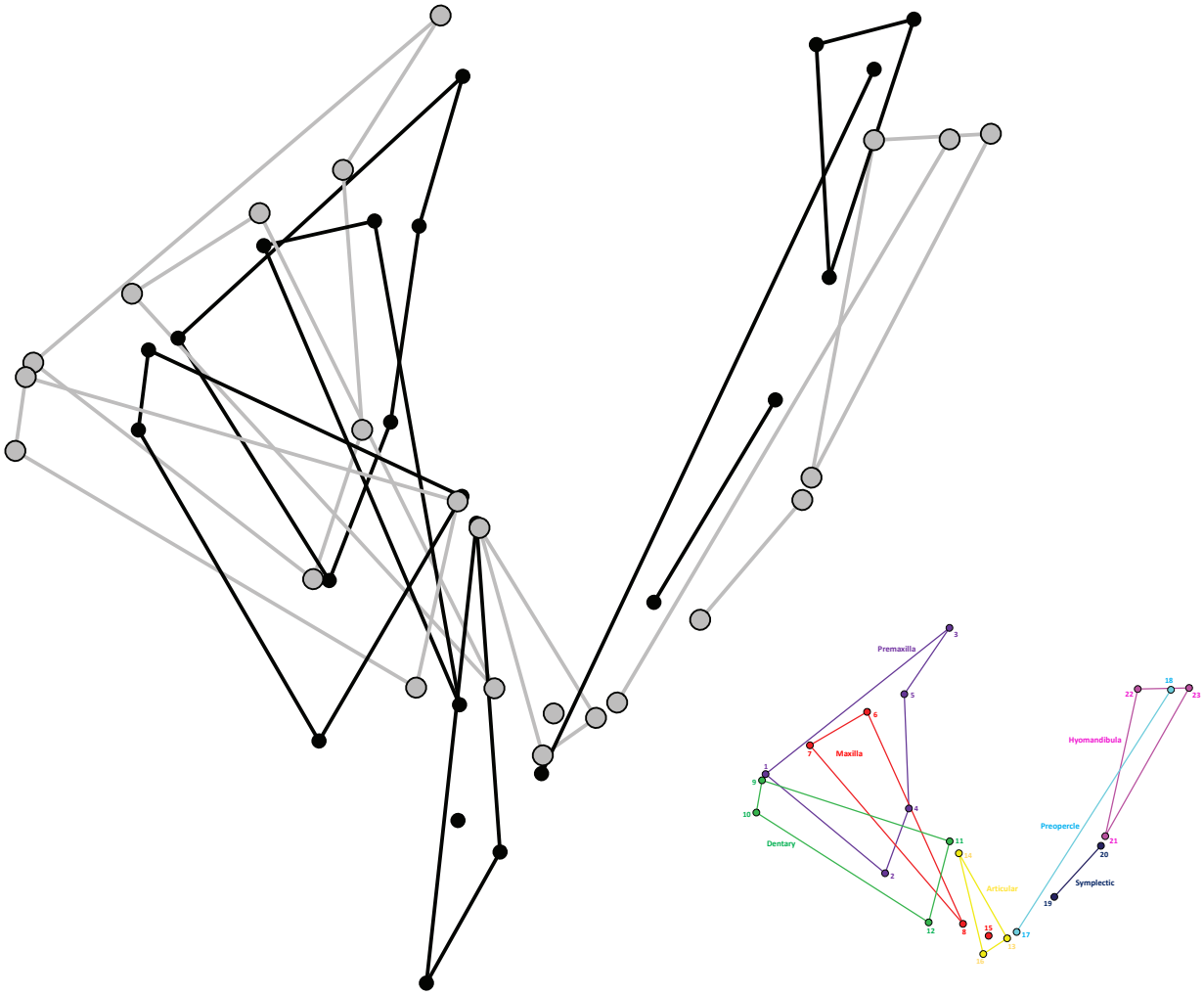

Figure 13. 2D Wireframe diagram of all 23 landmarks from principal component 1 (PC1). Grey colored wires show maximum variation (corresponding to *Parazen pacificus*) in the negative principal component direction, whereas black colored wires show the maximum variation (corresponding to *Zenopsis conchifer)* shown in the positive direction. Bottom right is a colored reference diagram model from Figure 11.

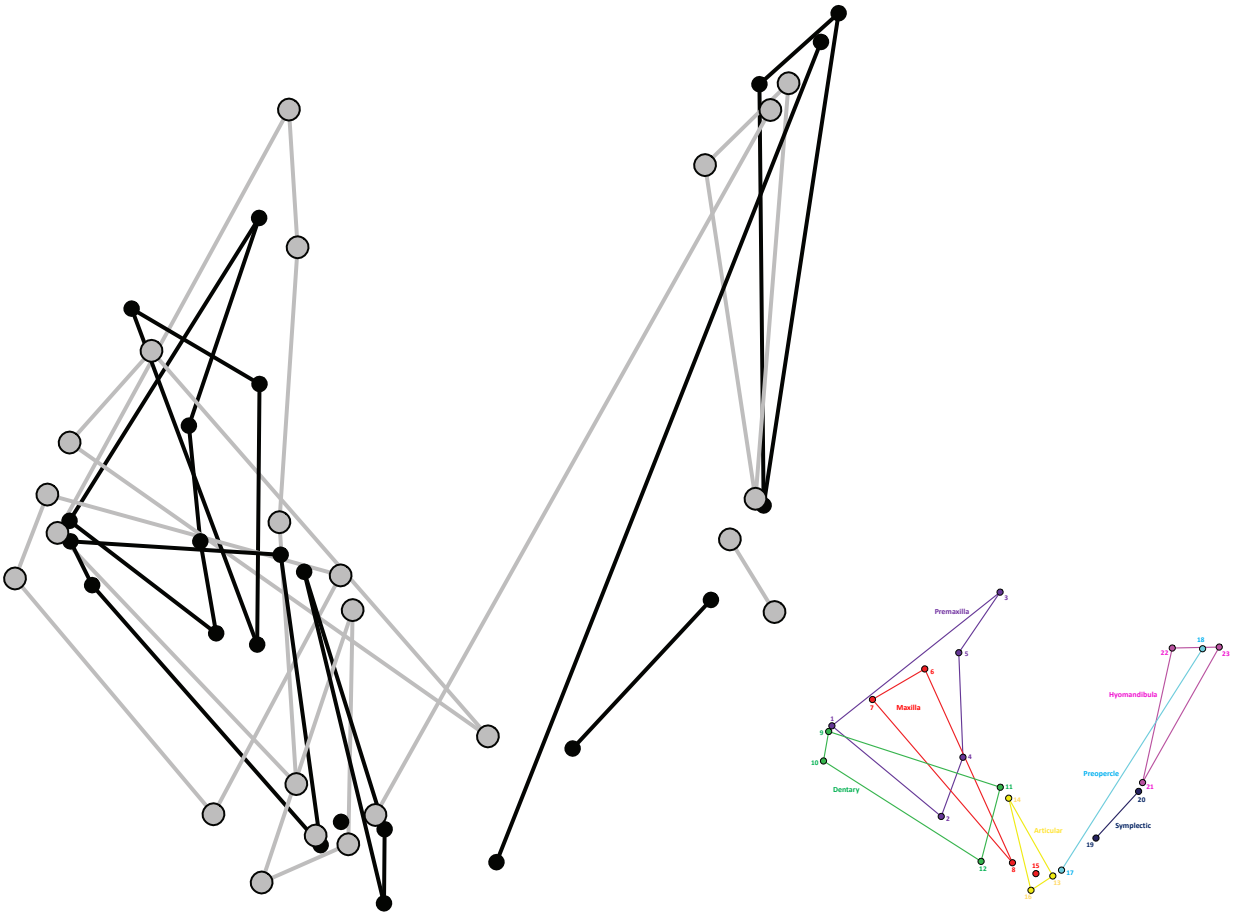

Figure 14. 2D Wireframe diagram of all 23 landmarks from principal component 2 (PC2). Grey colored wires show maximum variation (corresponding to *Zenion hololepis)* in the negative principal component direction, while black colored wires show the maximum variation (corresponding to *Xenolepidichthys dalgleishi)* shown in the positive direction. Bottom right is a colored reference diagram model from Figure 11.

Xenolepidichthys dalgleishi is indicative of the maximum variation in the positive direction for PC2, while *Zenion hololepis* shows the maximum variation in PC2 in the negative direction. *Cyttus australis* also lies close to the maximum extent of PC2 variation. The wireframe (Fig. 14) illustrates that the second principal component corresponds to a change in the length of the jaws with more minor differences seen in the individual bones of the anterior section. Furthermore, it still displays some trends seen in PC1, with the negative maximum variation of PC2 showing larger jaws, especially in the premaxilla and maxillary bones.

Stethopristes eos and *Parazen pacificus* show the maximum variation in the negative direction of PC3, while *Zenion hololepis* shows the maximum variation in the positive direction of PC3 (Fig. 15). The wireframes for principal component 3 (PC3) did not show significant changes in the size or shape of the upper and lower jaws but were able to capture significant variation in the bones of the suspensorium (Fig.16). Smaller changes were seen in the orientation of specific bones of the upper and lower jaws.

Wireframe diagrams for principal components 1-3 were created for each individual bone from the data set. These bones included the premaxilla, maxilla, dentary, articular, symplectic, preopercle, and hyomandibula. Premaxillary variation in size shifts from a larger and longer length at PC1 minimum to a shorter and slightly smaller premaxilla at PC1 maximum (Fig. 17). A clear decrease in the length and size of the premaxillary ascending process was observed. Furthermore, PC2 results for the first five landmarks corresponding to the premaxilla show a drastic decrease in the size and length of the premaxilla and its ascending process. This

indicates that *Zenion hololepis* displays larger jaws compared to *Xenolepidichthys dalgleishi,* with a much longer ascending process. PC3 was unable to capture any significant changes in the premaxillary bone shape and only showed slight changes in their orientation.

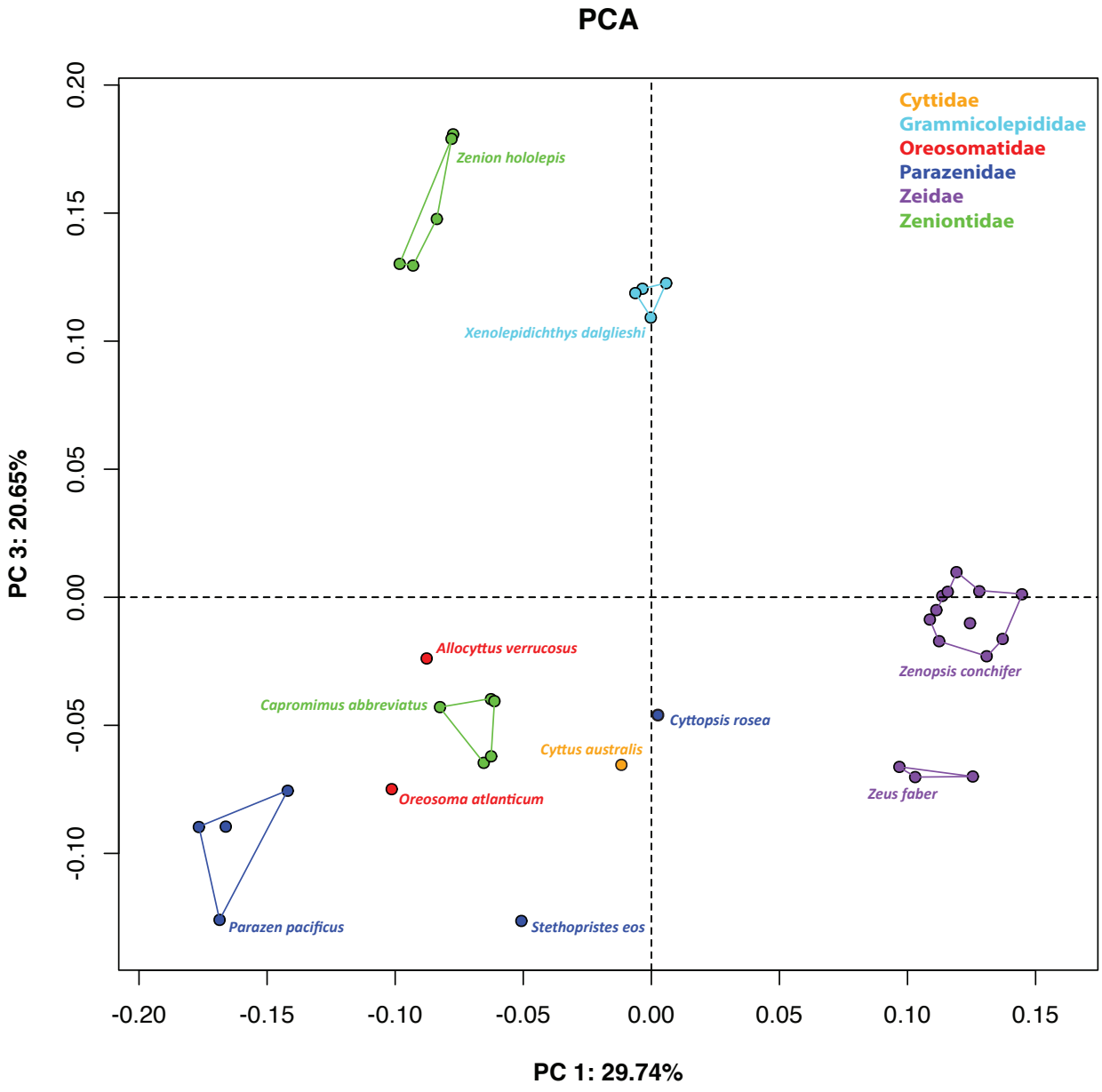

Figure 15. Principal Components Analysis Plot of all 23 landmarks done on 36 Zeiform specimens. The x-axis shows Principal Component 1 (PC1), while the y-axis displays Principal Component 2 (PC3). Each represented Zeiform family as originally recognized by Tyler et al. (2003) is specified by color.

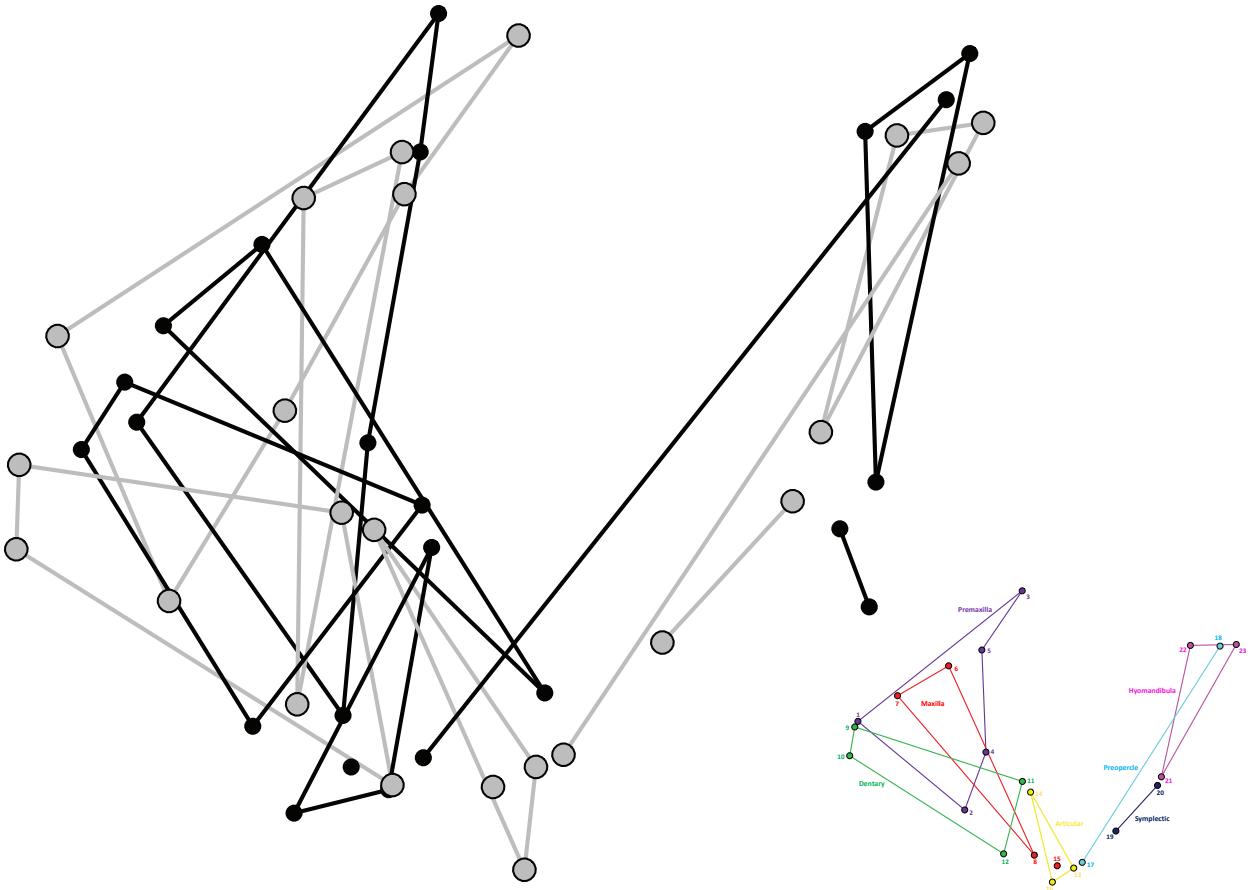

Figure 16. 2D Wireframe diagram of all 23 landmarks from principal component 3 (PC3). Grey colored wires show maximum variation (corresponding to *Stethopristes eos + Parazen pacificus)* in the negative principal component direction, while black colored wires show the maximum variation (corresponding to *Zenion hololepis)* shown in the positive direction. Bottom right is a colored reference diagram model from Figure 11.

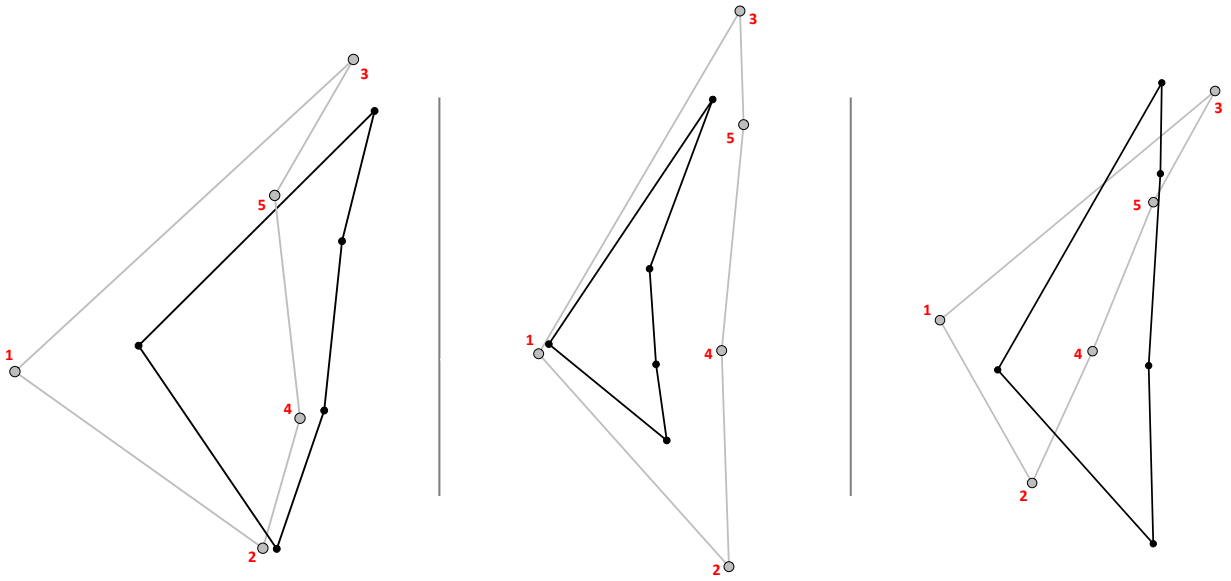

Figure 17. 2D Wireframe diagram of all 5 landmarks (numbered 1-5 in red color) on the premaxilla bone from PC1 (left), PC2 (middle), and PC3 (right). Grey colored wires show maximum variation in the negative principal component direction, while black colored wires show the maximum variation shown in the positive direction. Landmarks 1 and 3 correspond to the length of the ascending premaxillary process.

Wireframe diagrams for principal components 1-3 for all three landmarks of the maxilla capture a change in the orientation of the bone (Fig. 18). In PC1 and PC3 there is not a change in the size or shape of the maxilla, but rather a shift in the angle of the maxillary bone. PC2 captures a significant change in the size of the maxillary bone, with the minimum PC2 variations displaying a more vertical and longer shape and the maximum showing a decrease in size. As was observed in PC2 for the premaxillary landmarks, there is a large decrease in the size and length of the maxillary bone corresponding to *Zenion hololepis* and *Xenolepidichthys dalgleishi.* This illustrates a drastic variation in the maxilla and premaxilla of these two species; these two bones aid in upper jaw protrusion due to the four-bar linkage mechanism that we see in Zeiformes.

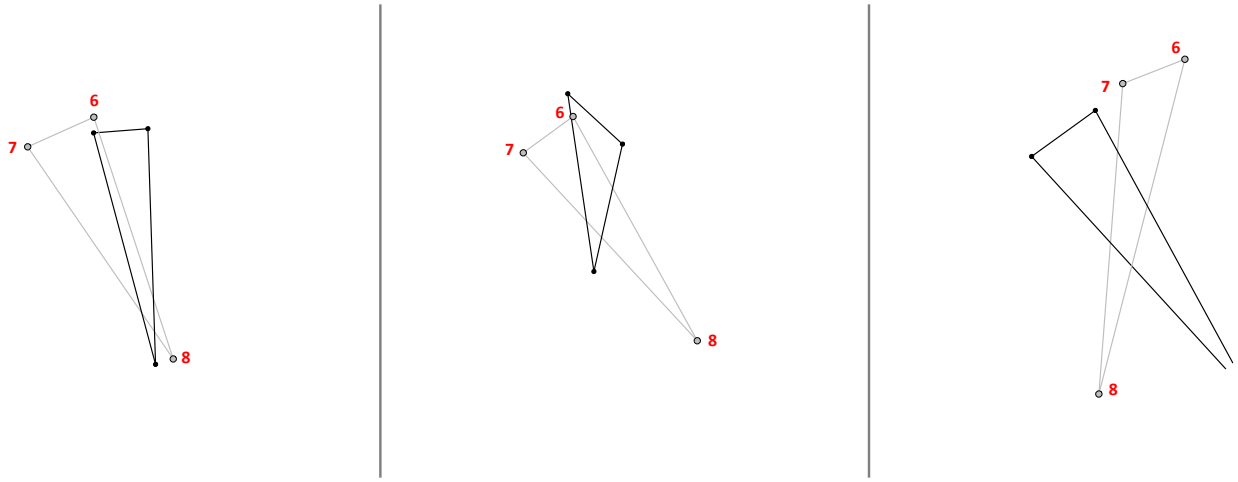

Figure 18. 2D Wireframe diagram of all 3 landmarks (numbered 6-8 in red color) on the maxillary bone from PC1 (left), PC2 (middle), and PC3 (right). Grey colored wires show maximum variation in the negative principal component direction, while black colored wires show the maximum variation shown in the positive direction.

The dentary and articular bones were landmarked to show variation in the lower jaw, which is the input linkage for the four-bar linkage feeding mechanism discussed in Chapter 1. Wireframe diagrams for principal component 1 of the dentary bone (Fig.19) illustrate a slight difference in length and width, with a significant change in the length of the articular bone (Fig. 20). Specifically, the PC1 minimum for *Parazen pacificus* shows longer and skinnier lower jaw bones versus the PC1 maximum for *Zenopsis conchifer*, which has shorter and more vertically taller jaws. Principal component 2 does not show a significant change in the size and shape of the dentary bone, but rather shows a drastic shift in the placement and length of the ventral flange of the dentary (landmark #11). Principal component 3 only displays slight changes to the size and the shape of the dentary bone.

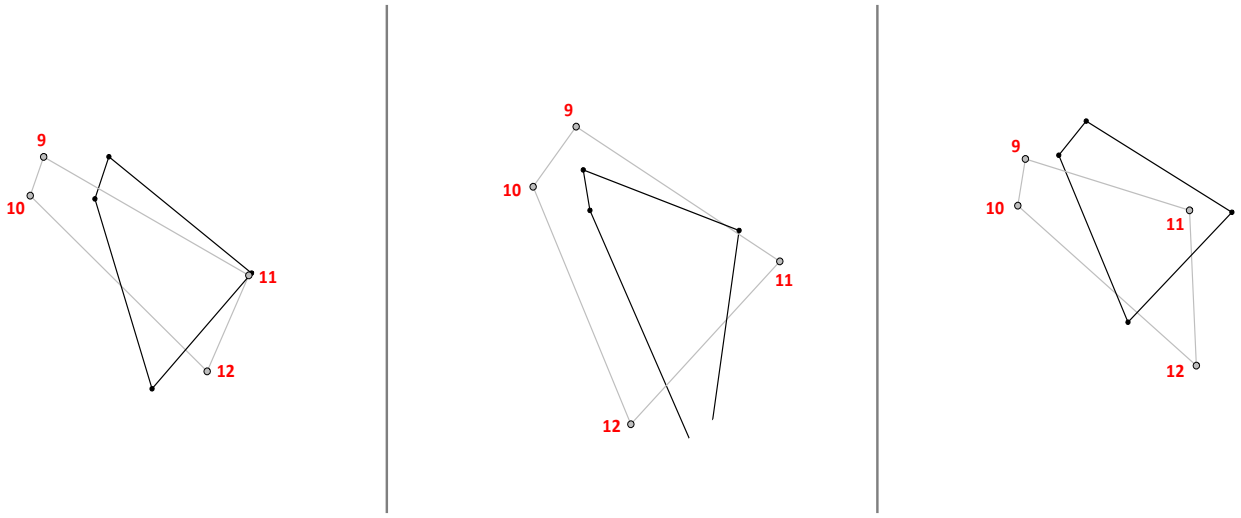

Figure 19. 2D Wireframe diagram of all 4 landmarks (numbered 9-12 in red color) on the dentary bone of the lower jaw from PC1 (left), PC2 (middle), and PC3 (right). Grey colored wires show maximum variation in the negative principal component direction, while black colored wires show the maximum variation shown in the positive direction.

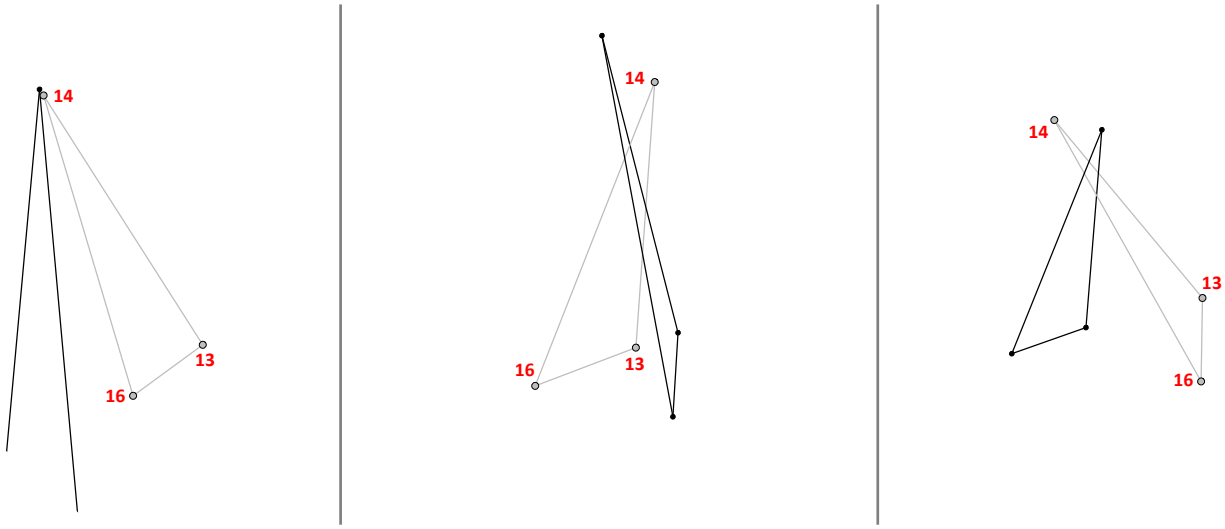

Figure 20. 2D Wireframe diagram of all 3 landmarks (numbered 13, 14, 16 in red color) on the articular bone of the lower jaw from PC1 (left), PC2 (middle), and PC3 (right). Grey colored wires show maximum variation in the negative principal component direction, while black colored wires show the maximum variation shown in the positive direction.

The symplectic, hyomandibula, and preopercle bones are all landmarked. The symplectic and hyomandibula make up an important part of the suspensorium that suspends the lower jaw to the neurocranium. There are notable changes in variation with respect to the size and length of the suspensorium bones in PC1. PC2 and PC3 did not illustrate any notable overall changes in size, but rather just a small shift in the orientation and shape. With respect to the individual bones of the suspensorium, only the hyomandibula showed significant changes to its size and orientation in PC1 (Fig. 21). Wireframes for the symplectic and preopercle bones did not show significant changes and only had small shifts in the orientation or the shapes of the bones (Fig. 22).

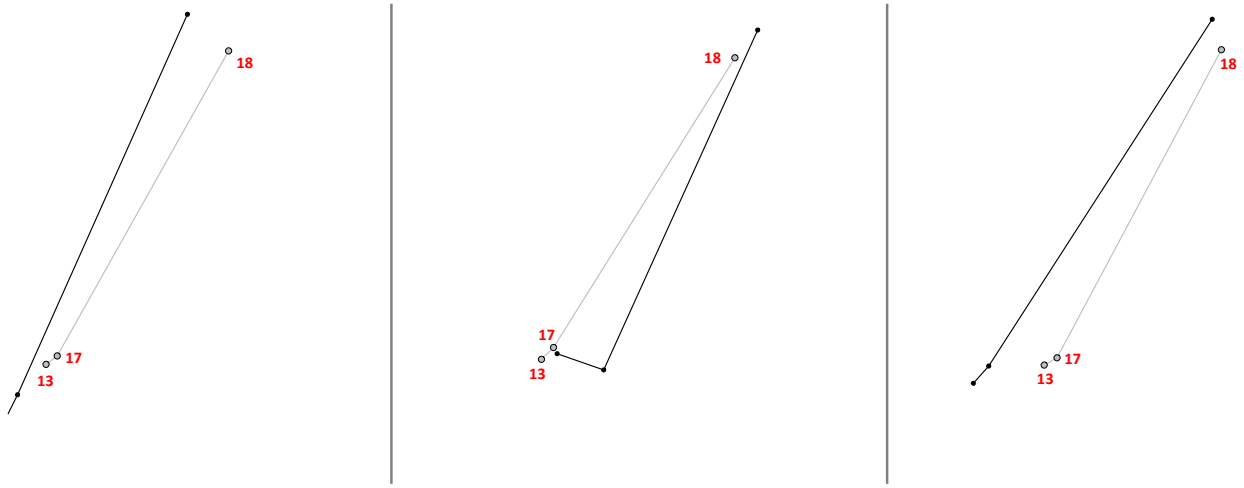

Figure 21. 2D Wireframe diagram of the 2 landmarks (numbered 17-18 in red color) on the preopercle bone of the suspensorium from PC1 (left), PC2 (middle), and PC3 (right). Grey colored wires show maximum variation in the negative principal component direction, while black colored wires show the maximum variation shown in the positive direction. Landmark 13 refers to the posterior extent of the articular and is illustrated to show the relative position to the lower jar.

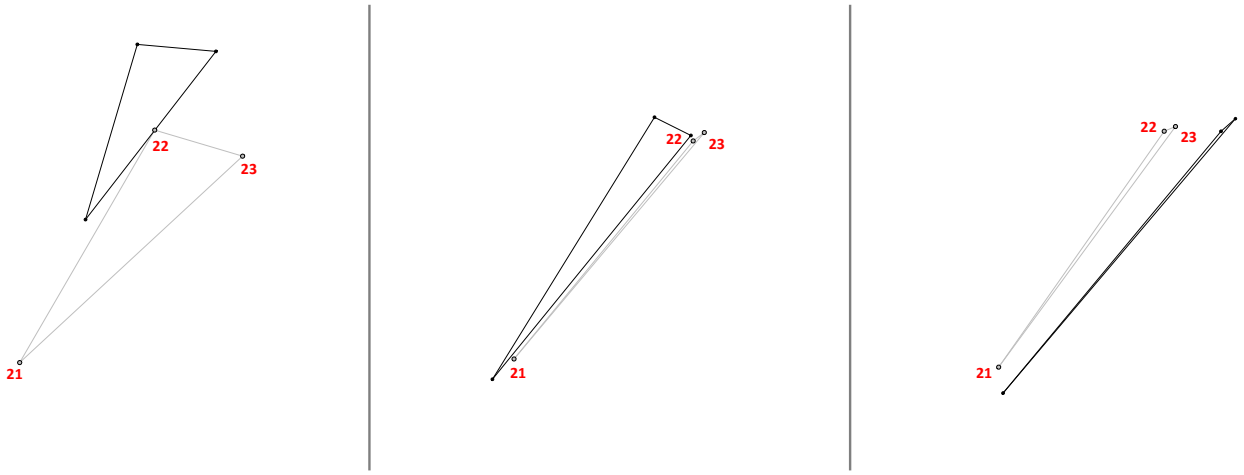

Figure 22. 2D Wireframe diagram of all 3 landmarks (numbered 21–23 in red color) on the hyomandibula bone of the suspensorium from PC1 (left), PC2 (middle), and PC3 (right). Grey colored wires show maximum variation in the negative principal component direction, while black colored wires show the maximum variation shown in the positive direction.

The present wireframe diagrams were able to show interesting overall variation among the principal components and individual fish species. Furthermore, some principal components that did not indicate significant changes in the entire jaw did reveal changes in individual bones that made up the upper jaw, lower jaw, and the suspensorium. Overall, principal component 1 captures the greatest amount of jaw variation, showing a shift from longer and more slender jaws in species such as *Parazen pacificus* to shorter, more vertically taller jaws in species such as *Zenopsis conchifer*. Not much variation in seen in the size and shape of specific jaw bones, but rather an overall shape change trend is observed. Principal component 2 was able to capture a significant change in the size of the anterior portion of the jaws and skull. It also illustrated large shifts in the size of the upper jaw bones, especially in the size of the premaxillary bone. Although it was more difficult to visualize significant changes in the size and shape of the lower jaw bones together, it was possible to see large variation in the individual dentary and articular

bones. Principal component 3 was able to capture some significant variation in the size and shape of the bones of the suspensorium.

OBJECTIVE TWO

(Testing similarities and differences to Grande et al., 2018)

Phylomorphospace Comparison

The phylomorphospace analysis (combined-evidence tree from Grande et al., 2018 mapped into the PCA morphospace; Fig. 23) suggests that the common ancestor of extant zeiforms was one with near-average jaw morphology. This study recovers a similar concentration of lineage branching near the center (0, 0) of the morphospace as is seen in the Grande et al. (2018) body-form phylomorphospace. This branching near the center of the phylomorphospace is consistent with the short branches near the base of the zeiform radiation in the phylogenetic tree (Fig. 4). Both phylomorphospaces were created using the same combined-evidence phylogeny from Grande et al. (2018: fig. 7). There are at least four divergent lineages that radiate in different directions of change (Fig. 23), with two cases of convergence between zeiform taxa. The first of these is seen between *Stethopristes eos* and *Cyttus australis*, and the second case involves Oreosomatidae and *Parazen pacificus.* The present phylomorphospace mostly agrees with that of Grande et al. (2018), but with a few relationships that differ, such as those of Parazenidae and Zeniontidae.

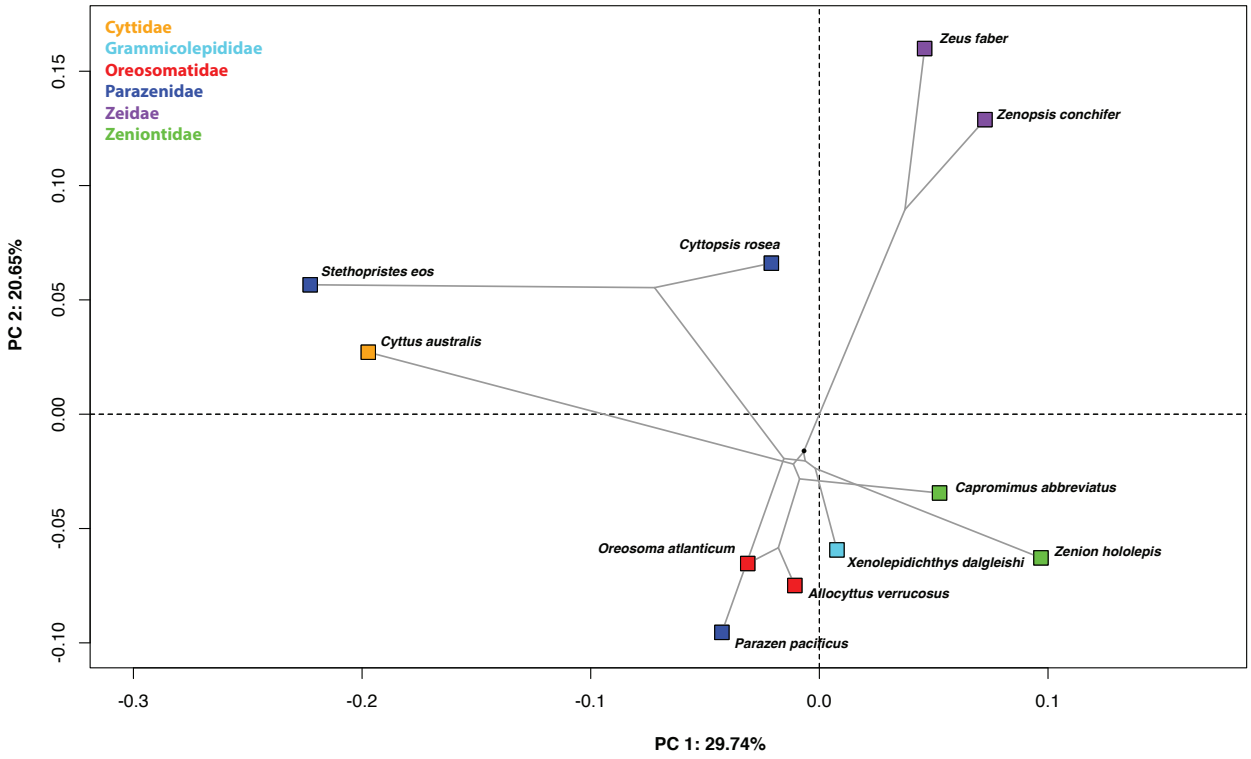

Figure 23. Combined-Evidence Phylomorphospace - Morphometric analysis of averages for 11 species plotted against the molecular and morphological phylogenetic results obtained from Figure 4. The phylomorphospace diagram shows variation in the morphospace defined by the first two principal components. Each color represents one of the six original families of Tyler et al. (2003): Zeidae (Purple), Zeniontidae (Green; not monophyletic in Grande et al. 2018), Parazenidae (Blue), Oreosomatidae (Red), Cyttidae (Orange), and Grammicolepididae (Teal). The black circle near the center of the morphospace (0,0) denotes the root of the phylogeny. The orientation of the diagram appears different than in Figures 11 and 14 because Figure 23 is based on species averages, rather than individual specimens, causing a rotation of the morphospace in Figure 23. However, relative distances among points are similar.

The phylomorphospace supports the monophyletic relationship of the family Zeidae, which is the earliest diverging lineage of Zeiformes, with the species showing a recent divergence from a shared ancestor in their overall jaw morphology but remaining relatively similar. This group specifically illustrates a morphological trend towards dorsoventrally longer

and taller jaws, especially with the length of their suspensorium. They also display large upper jaw bones, which allows this group to have extensive upper jaw protrusion.

With respect to the family Zeniontidae (represented by *Zenion* and *Capromimus* in this analysis), the combined evidence phylogeny of Grande et al. (2018) did not recover this taxon as monophyletic, and the two genera did not exhibit significant convergence in body form. However, in the present phylomorphospace, the two genera are seen to be convergent in jaw morphology. Both show significant upper jaw protrusion due to the large size of their upper jaw bones. They also display dorsoventrally more slender and more anteriorly extended jaws. This trend was evident for *Zenion hololepis* in Grande et al. (2018), with that species showing more oblique mouths and shallower bodies than most other taxa in the order.

Grande et al. (2018) did not find Grammicolepidae, as previously proposed to include *Macrurocyttus*, to be monophyletic. Grande et al. (2018) removed *Macrurocyttus* and retained only *Grammicolepis* and *Xenolepidichthys* in the family. The present study could not examine this question as only *Xenolepidichthys dalgleishi* was available, and it showed a slight convergence with the oreosomatids. *Xenolepidichthys* showed the maximum variation in the positive direction for PC2. This was a trend towards overall smaller jaws, especially with respect to the upper jaw bones. This group is expected to show the least amount of jaw protrusion amongst extant Zeiform taxa. The Cyttidae were another family for which only one representative was available, and that species (*Cyttus australis*) showed a slight convergence with *Stethopristes eos*, which is not closely related. *Cyttus australis* also showed similar jaw morphology to *Xenolepidichthys dalgleishi,* with smaller jaws and less upper jaw protrusion.

The family Parazenidae was one that Grande et al. (2018) supported as monophyletic in their combined evidence and their Bayesian molecular phylogenies, though not in their maximum likelihood molecular results. However, their phylomorphospace found strongly divergent trends for the lineages of this group (*Parazen*, *Cyttopsis*, and *Stethopristes*). The present phylomorphospace does the exact same thing: the three represented genera of Parazenidae diverge strongly from each other in terms of their jaw morphology. Furthermore, *Parazen pacificus* shows a convergence with Oreosomatidae in the present jaw phylomorphospace (Fig. 23), whereas in body form *Parazen* was convergent with *Zenion* in the results of Grande et al. (2018). Oreosomatidae showed more average-sized jaws, with notable upper jaw protrusion due to the increased size of their upper jaw bones. This family needs more representation in analyses because they show the fastest evolving taxa and shortest branch lengths in their phylogeny. Unfortunately, they are more difficult to find in museum collections, so we were only able to use two intact specimens.

CHAPTER FOUR

DISCUSSION

Previous research conducted on zeiform morphology (Tyler et al., 2003; Grande et al., 2018) looked at overall body shape variation and differences in morphological character traits. Using morphospace data for body form, Grande et al. (2018) found that the early radiation of zeiforms involved several initial lineage splits, but also showed major divergences among the main lineages. Zeiformes have shown great variation in terms of overall body shape and morphological characters, but until now, no research has used updated 3D morphometric techniques to look specifically at the bizarre zeiform jaw morphology as a novel character set. This study has thus placed an emphasis on jaw morphology to help resolve some phylogenetic relationships and patterns seen within the apparent rapid radiation of zeiform fishes. This thesis had two main sections: (1) Exploration of extant zeiform taxa using 3D geometric morphometrics techniques to better understand their jaw morphology and evolution. (2) Comparison of phylomorphospace data to that of Grande et al. (2018) and examination of evolutionary patterns of divergence and convergence.

Geometric Morphometrics

The phylomorphospace analysis of this study suggests that the early radiation of zeiforms involved several initial lineage splits of fishes with near-average jaw morphology, as indicated also by the short branch lengths seen in the phylogeny of Grande et al. (2018). This result resembles the body-form phylomorphospace results of Grande et al. (2018), but this time focused

on jaws. *Zeus* and *Zenopsis* are an early diverging lineage from the common ancestor of all extant Zeiformes. Jaw protrusion had already evolved in an earlier zeiform ancestor, and then the lineages diverged, leading to a wide range of premaxillary protrusion capabilities in the extant Zeiformes. Furthermore, there are two examples of convergences that are illustrated by a radiation from this average morphotype. One of these convergences led to two genera (*Stethopristes* and *Cyttus*), with relatively smaller upper jaw bones compared to other taxa but longer and vertically taller suspensorium and posterior jaw bones. The second convergence was also between two genera (*Oreosoma* and *Parazen*), which display larger upper and lower jaw bones, and relatively longer suspensorium and posterior jaw bones. In the PC2 analysis of the upper jaw, a drastic divergence of *Zenion* and *Xenolepidichthys* with respect to premaxillary size and the length of the ascending process was observed. The longer jaw size and increased length of the ascending process allows individuals of *Zenion* to slide their upper jaws more anteriorly than *Xenolepidichthys* and increase their jaw protrusibility. A majority of zeiform taxa were occupying the negative PC1 morphospace, which displayed a pattern of larger and more protrusible jaws. This evolutionary trend of larger and more protrusible jaws could be an important factor in their evolutionary success and could have allowed them to capture more elusive prey in their respective habitats.

The goal of this study was to explore zeiform taxa using a novel character set (i.e., jaw morphology) to see if it could resolve some of their interrelationships and show evolutionary trends within the order. To do so, the phylomorphospace based on jaws was compared to that of Grande et al. (2018) based on body form. The present morphospace based on jaws showed very similar initial lineage radiations indicative of the short branch lengths that can be seen in the

combined evidence phylogeny from Grande et al. (2018). Furthermore, many genera occupied similar areas of the morphospace. Most of the morphospace agrees with that of Grande et al. (2018), but Parazenidae and Zeniontidae revealed new relationships and evolutionary trends that did not agree with previous research. These two groups have been recovered as non-monophyletic in the past, Parazenidae by Tyler and Santini (2005), and Zeniontidae in the combined-data results by Grande et al. (2018).

The combined-evidence molecular and morphological phylogeny (Fig. 4) that was used here for the phylomorphospace recovered Zeniontidae as non-monophyletic. The present phylomorphospace based on jaws showed a strong convergence between *Capromimus abbreviatus* and *Zenion hololepis*, which could mean that these species are more similar when looking at their jaws instead of body shape. This group seems to have evolved similar jaw morphology, which could be due to occupying similar habitats and feeding on similar diets. This group appears closely related in Tyler et al. (2003), Tyler and Santini (2005), and Grande et al. (2018) morphological analyses only, meaning that this family is probably held together more by its morphology than its molecular makeup. This can be seen in the Grande et al. (2018) morphospace (Fig. 24), where *Zenion* seems to diverge from *Capromimus* and *Cyttomimus.*

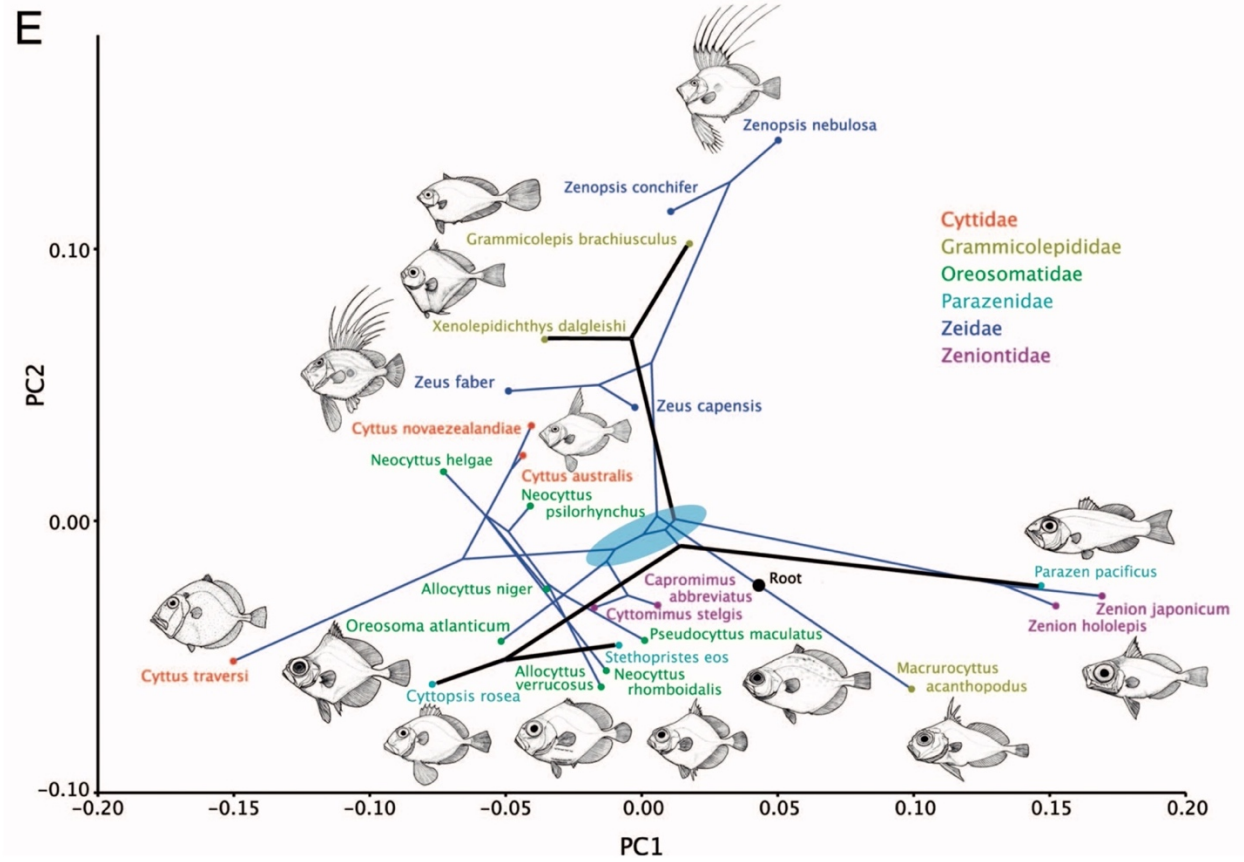

Figure 24. Grande et al. (2018) Combined-Evidence Phylomorphospace - Phylomorphospace diagram showing variation in the morphospace defined by the first two principal components, with the combined phylogeny of Figure 4 mapped into the morphospace. Thin blue lines and thick black lines represent convergent lineages. Note that most of the major lineages arose from common ancestors with near-average morphologies (blue ellipse). Thumbnail drawings by Michael Hanson.

Monophyly of Parazenidae has been debated over the years and the relevant taxa still have not been fully resolved. Grande et al. (2018) found this group to be monophyletic in their combined evidence phylogeny, but saw a divergence of *Parazen*, *Cyttopsis*, and *Stethopristes* in their morphospace. The present jaw-based phylomorphospace saw a similar radiating divergence of the three genera, where *Parazen* converges with the oreosomatids and *Stethopristes* converges

with *Cyttus*. Monophyly of *Parazenidae* is only supported by one morphological synapomorphy and four other characters that exhibit homoplasy (Tyler et al., 2003). The synapomorphy is having one anal fin spine; most of the similar traits for this family have to do with spine arrangement and spiny rays. The support of these characters in all four analyses performed by Tyler et. al. (2003) showed weak to good support. This is the lowest level of support for all clades of Zeiformes. Tyler and Santini (2005) found that Parazenidae were not monophyletic, with *Parazen* needing further investigation and information. Moreover, *Parazen* was found to be in a polytomy with Zeniontidae and not recovered with the other two taxa in its clade.

In Grande et al. (2018), Parazenidae are monophyletic in the combined evidence phylogeny and both morphology-only cladograms but were not closely related in molecular-only results shown in the maximum likelihood and Bayesian inference cladograms. Once again, these results, as with that of Tyler et al. (2003), provide only weak support for the monophyly of this clade. On molecular evidence this clade is not recovered as monophyletic, and we only see them being closely related when morphological data are involved. In summary, this group may not be as closely related as they appear at first, but rather convergent in some morphological traits.

Variation in Zeiform Morphology

The amount of morphological variation among zeiform fishes is extraordinary (Figs. 5, 23). As discussed earlier, the phylogenetic results of Grande et al. (2018) indicated a rapid radiation and diversification among zeiform families, as evidenced by short branch lengths near the base of the phylogenetic zeiform tree (Grande et al., 2018). This radiation gave rise to significant morphological disparity among groups of zeiforms, even though they began their histories with only minor molecular and morphological differences.

Modularity has been targeted as a primary evolutionary phenomenon facilitating the evolvability of complex systems. Complex morphological systems are subject to constraints that divide the phenotype into modules (i.e., discrete units of variation), which influence their developmental and evolutionary trajectories (Duclos et al., 2021). Broadly speaking, modularity is considered a foundational mechanism for morphological and evolutionary variation, because of the capacity for morphological and/or developmental systems to behave as quasi-independent units. Usually, modularity is invoked in the context of variational modularity, where modules are networks of interacting elements behaving as highly integrated traits (i.e., traits that are strongly correlated). The modules covary strongly internally, but weakly with other sets of elements (other modules), and thus often act as discrete units of variation.

Complex and highly variable phenotypes can thus be decomposed into modules. Modularity allows morphological or developmental systems to vary or evolve quasi-independently of other systems, allowing for phenotypic space to be explored while reducing the risk that adapted systems become maladapted as a result of covariation (Duclos et al., 2021). This modular partitioning is thought to promote disparity among developmental and evolutionary trajectories, and its recognition allows enhanced understanding of evolutionary processes.

Modularity of zeiform jaw structures and possible sub-modularity of portions of the zeiform jaw module could have facilitated their rapid evolution and could have been partly responsible for the great diversity, evolutionary success, and longevity of the order.

The study of Grande et al. (2018) identified a radiation of zeiform body plans from a less modified, ancestral starting point. The present study identifies a radiation of zeiform jaw morphologies, also from a less modified starting point. But, interestingly, the trajectories of the

radiating lineages are not always the same between body forms and jaws. There are examples of convergences and divergences in both, but two taxa that converge in one might diverge in the other, and vice versa.

Very likely, it is the modularity of zeiform morphology and developmental constraints that is at the root of this phenomenon. Body form responds to one or more sets of selective pressures and constraints, while jaws respond to mostly different sets of selective pressures and constraints. Their developmental mechanisms are also rather different. In this way, the extraordinary diversity and disparity of zeiform fishes can be partly explained by bodies and jaws belonging to different evolutionary modules.

Jaw morphology as a variational module has been explored with respect to the adaptive radiation of African cichlids. Parsons (2011) proposed the decoupling of the oral and pharyngeal jaws, thereby creating submodules within the entire craniofacial area. If this is the case, and each submodule responded to different selection pressures resulting in shifts in developmental timing between the two (i.e., heterochrony), this might help to explain the enormous amount of variation and specialization among African cichlids. Like these cichlids, zeiform taxa also show considerable variation among taxa with respect to specific bones of the jaws, possibly the result of submodulization and heterochronic shifts in development within the entire craniofacial area. It is thus hypothesized here that modularity of the jaw in zeiform taxa may have influenced their rapid and successful radiation as seen in the short, deeper branch lengths of the phylogeny, the strong divergences of lineages, and the examples of unrelated lineages converging on similar jaw morphologies.

Future Directions

With the new phylogenetic placement of zeiforms within Paracanthopterygii, the interrelationships of this taxon needed some further research. While Grande et al. (2018) were able to offer a new comprehensive look at this order with total body morphological and molecular data, this study explored a smaller subset of morphological characters by looking at their jaws in a 3D analysis. With newer technology, we have seen a huge expansion of methods for 3D geometric morphometric scanning techniques and analyses. Although a 3D micro-CT scanner was used for this study, it is not available to all scientists looking to explore these types of data sets. Marcy et al. (2018) illustrates the repeatability and similarities between micro-CT scanning and 3D surface scanning, which could offer an alternative that is much easier to access and less costly.

Although the data set that was used for this study did represent all extant zeiform families, it was unable to include all genera or multiple specimens for each genus. Specifically, the oreosomatids were the most difficult family to find enough intact specimens through museum collections. This group is of great importance and needs further resolution of their evolutionary radiation that can be seen by their short branch lengths. Further research needs to be conducted on their morphology and molecular data that can hopefully include a greater sample size of specimens for best repeatability. Another group that needs further investigating is Parazenidae, which had contrasting results in this study to previous work. Overall, this study was able to offer new methods for 3D geometric morphometric studies and has revealed new evolutionary insight into the complex relationships of zeiforms. The best next steps are to gather research on their

habitat patterns and diets. With that type of information, we can start looking at specific novel characters that will lead to ecological trends and help us better understand the rapid radiation and evolutionary success of this clade of fishes.

APPENDIX A

REFERENCE MATERIAL

Reference Specimens

All reference material were cleared and stained (CS) specimens preserved in 80% glycerin.

Institutional abbreviations: FMNH, Field Museum of Natural History; KU, University of Kansas Museum of Natural History; LACM, Natural History Museum of Los Angeles County; MCZ, Museum of Comparative Zoology; USNM, Smithsonian National Museum of Natural History.

Parazenidae.—Parazen pacificus: 1 specimen, 95.2mm SL: FMNH 67158.

Cyttopsis rosea: 1 specimen, 78mm SL: FMNH 67091.

Zeidae.—Zenopsis conchifer: 1 specimen, 42.3mm SL: FMNH 67179.

Zeus faber: 1 specimen, 76.00mm SL: USNM 307842.

APPENDIX B

CODING MATERIAL

R Coding Text

```
library(geomorph)
library(Morpho)
library(ggplot2)
library(ape)
library(abind)

setwd("~/Desktop/3D Coordinates")

# read in data
{
 filelist <- list.files(pattern = "*.txt")

 # list all morpholgika files - lists all txt files with that extension.
 filelist
 #create multi function - homegrown function to read my morphologika files and coordinates
extracted
 read.multi.morphologika <- function(filelist){
  names <- gsub (".txt", "", filelist)
  coords <- NULL
  k <- dim(read.morphologika(filelist[1]))[1]
  for (i in 1:length(filelist)){
   temp <- read.morphologika(filelist[i])
   coords <- rbind(coords, two.d.array(temp)) }
  raw.Y <- arrayspecs(coords, k, 3)
  dimnames(raw.Y)[[3]] <- names
  return(raw.Y)}
```

```
 #create object of data
 mydata<-read.multi.morphologika(filelist)
}

mydata[,,13] #reading the 13th specimen

for (i in 1:23)
{
 mydata[i,3,13]<- -mydata[i,3,13]
} #flipping

#procrustes fit
gpa1<- gpagen(mydata, ProcD=T)


mydata
#create meta - creating metadata from lists to string
{
 nms <- dimnames(mydata)[[3]]
 nms
 meta<-NULL
 library(stringr)
 meta <- str_match(nms, "(([A-Z][a-z]+)(_[a-z]+)+(_[a-z]+)?)_(\\d+)")
 meta
 meta <- as.data.frame(meta[,c(3,4,6)])
```

```
  names(meta) <- c("Genus", "Species", "num")
  meta
}
summary(meta)

write.csv(unique(meta$Species), file = "speciesnames.csv")
Csize<-gpa1$Csize
Csize<-as.matrix(Csize)
size<-Csize[1:124]
length(gpa1$Csize)

gdf <- geomorph.data.frame(coords = gpa1$coords, Genus=meta$Genus, Species=meta$Species,
Number=meta$num)
gdf
PCA <- gm.prcomp(gdf$coords, phy = NULL, align.to.phy = FALSE, GLS = FALSE, transform
= FALSE)

PCA <- gm.prcomp(gdf$coords)
summary(PCA)
Colours<-gdf$Species
Colours[which(Colours=="_verrucosus")]<-"pink"
Colours[which(Colours=="_abbreviatus")]<-"turquoise"
Colours[which(Colours=="_rosea")]<-"grey"
Colours[which(Colours=="_australis")]<-"lightgreen"
Colours[which(Colours=="_atlanticum")]<-"purple"
Colours[which(Colours=="_pacificus")]<-"orange"
Colours[which(Colours=="_eos")]<-"lightblue"
```

```
Colours[which(Colours=="_dalgleishi")]<-"red"
Colours[which(Colours=="_hololepis")]<-"brown"
Colours[which(Colours=="_conchifer")]<-"darkgreen"
Colours[which(Colours=="_faber")]<-"coral4"
plot(PCA, axis1 = 1, axis2 = 2, main = "PCA", pch = 21, bg = Colours, cex = 1, cex.lab = 1,
font.lab = 2) #PCA1 vs 2
plot(PCA, axis1 = 1, axis2 = 3, main = "PCA", pch = 21, bg = Colours, cex = 1, cex.lab = 1,
font.lab = 2) #PCA1 vs. 3
plot(PCA, axis1 = 2, axis2 = 3, main = "PCA", pch = 21, bg = Colours, cex = 1, cex.lab = 1,
font.lab = 2) #PCA2 vs. 3

# Phylo PCA without projecting untransformed residuals
#Here, the phylogeny IS considered during the analytical step of the ordination, as the principal
components analysis is in this case calculated based on GLS-centering and projection of the data.
For details on the analytical part of this method, see Revell 2009, Evolution 63: 3258 - 3268;
Polly et al 2013, Hystrix 24: 33 - 41; Collyer & Adams, submitted.
phylo.PCA <- gm.prcomp(gdfavsp$coords, phy = tree, GLS = TRUE, align.to.phy = TRUE)
summary(phylo.PCA)
plot(phylo.PCA, phylo = TRUE, main = "phylo PCA")
#3D PCA Plot with a phylogeny and time on the z-axis (Use this one for all of my
phylomorphospaces)
plot(PCA.w.phylo, time.plot = TRUE, pch = 22, bg = c(rep("red", 2), rep("green", 1),
rep("orange", 1), rep("blue", 3), rep("yellow", 1), rep("green", 1), rep("purple", 2)), cex = 2,
    phylo.par = list(edge.color = "grey60", edge.width = 1.5, tip.txt.cex = 0.75,
                node.labels = F, anc.states = F))
```

```
plot(phylo.PCA, time.plot = TRUE, pch = 22, bg = c(rep("red", 2), rep("green", 1), rep("orange",
1), rep("blue", 3), rep("yellow", 1), rep("green", 1), rep("purple", 2)), cex = 2,
    phylo.par = list(edge.color = "grey60", edge.width = 1.5, tip.txt.cex = 0.75,
                     node.labels = F, anc.states = F))

plot(phylo.tPCA, time.plot = TRUE, pch = 22, bg = c(rep("red", 2), rep("green", 1),
rep("orange", 1), rep("blue", 3), rep("yellow", 1), rep("green", 1), rep("purple", 2)), cex = 2,
    phylo.par = list(edge.color = "grey60", edge.width = 1.5, tip.txt.cex = 0.75,
                     node.labels = F, anc.states = F))



#S3 method for gm.prcomp
plot(
  gdf,
  axis1 = 1,
  axis2 = 2,
  flip = NULL,
  phylo = FALSE,
  time.plot = FALSE,
  phylo.par = list(tip.labels = TRUE, node.labels = TRUE, anc.states = TRUE, node.pch =
                     21, node.bg = "grey", node.cex = 1, edge.color = "black", edge.width = 1, tip.txt.cex
                   = 1, tip.txt.col = "black", tip.txt.adj = c(-0.1, -0.1), node.txt.cex = 1,
                   node.txt.col = "grey", node.txt.adj = c(-0.1, -0.1)),
)

summary.gm.prcomp
```

```
#calculating average shapes using mshape
avverrucosus<-(gdf$coords[,,which(meta$Species=="_verrucosus")])
avatlanticum<-(gdf$coords[,,which(meta$Species=="_atlanticum")])
avabbreviatus<-mshape(gdf$coords[,,which(meta$Species=="_abbreviatus")])
avaustralis<-(gdf$coords[,,which(meta$Species=="_australis")])
avrosea<-(gdf$coords[,,which(meta$Species=="_rosea")])
aveos<-(gdf$coords[,,which(meta$Species=="_eos")])
avpacificus<-mshape(gdf$coords[,,which(meta$Species=="_pacificus")])
avdalgleishi<-mshape(gdf$coords[,,which(meta$Species=="_dalgleishi")])
avhololepis<-mshape(gdf$coords[,,which(meta$Species=="_hololepis")])
avconchifer<-mshape(gdf$coords[,,which(meta$Species=="_conchifer")])
avfaber<-mshape(gdf$coords[,,which(meta$Species=="_faber")])

dim(avverrucosus);dim(avatlanticum);dim(avabbreviatus);dim(avaustralis);dim(avrosea);dim(av
eos);dim(avpacificus);dim(avdalgleishi);dim(avhololepis);dim(avconchifer);dim(avfaber)
#should all be equal at 23 3

#creating an empty array of size 23 3 10
emptydf <- rep(NaN, 23*3*11)
avcoords <- array(emptydf, c(23, 3, 11))
dim(avcoords) #should be 23 3 10

dimnames(avcoords)[[3]] <- gdftips

#creating a list of average shapes for the loop
avlist<-list(avverrucosus,avatlanticum,avabbreviatus,avaustralis,avrosea,aveos,avpacificus,
        avdalgleishi,avhololepis,avconchifer,avfaber)
```

```
#Using a for loop to fill the empty array with the average shapes
for(i in 1:11){
  avcoords[,,i]<-avlist[[i]]
}
avcoords #there should be no NaNs anymore.

#Making the average geomorph dataframe
gdfavsp <- geomorph.data.frame(coords = avcoords, Species=gdftips)

gdfavsp

#tree files
#combined bayesian morphological + molecular
tree<-read.nexus(file="MrB combo ingroup only for morpho mapping.tre")

#Changing the names back to the original, getting matrix error from "remove"
tree$tip.label<-as.vector(c( "Allocyttus_folletti", "Allocyttus_verrucosus", "Allocyttus_niger",
"Neocyttus_helgae", "Neocyttus_rhomboidalis", "Neocyttus_psilorhynchus",
"Pseudocyttus_maculatus", "Oreosoma_atlanticum", "Capromimus_abbreviatus",
"Cyttomimus_stelgis", "Cyttus_australis", "Cyttus_novaezealandiae", "Cyttus_traversi",
"Cyttopsis_rosea", "Stethopristes_eos", "Parazen_pacificus1", "Parazen_pacificus",
"Grammicolepis_brachiusculus", "Xenolepidichthys_dalgleishi", "Zenion_hololepis1", "Cmaff",
"Zenion_japonicus", "Zenion_hololepis", "Zenopsis_conchifer", "Zenopsis_nebulosa",
"Zeus_capensis", "Zeus_faber", "Macrurocyttus_acanthopodus") ) #replaced all current tree tip
labels with new names
```

```
gdftips<-as.vector(c(
"Allocyttus_verrucosus","Oreosoma_atlanticum","Capromimus_abbreviatus","Cyttus_australis",
"Cyttopsis_rosea", "Stethopristes_eos", "Parazen_pacificus","Xenolepidichthys_dalgleishi",
"Zenion_hololepis",  "Zenopsis_conchifer", "Zeus_faber") ) #replaced all current tree tip labels
with new names

tree<- drop.tip(tree, setdiff(tree$tip.label, gdftips))
plot(drop.tip(tree, setdiff(tree$tip.label, gdftips)))#drop tips not represented in data
plot(tree)




#combined maximum likelihood tree
tree<-read.nexus(file="ML_zeif_13July.best.pruned.tre")

tree$tip.label<-as.vector(c( "Neocyttus_psilorhynchus", "Neocyttus_psilorhynchus",
"Neocyttus_helgae", "Neocyttus_helgae", "Neocyttus_rhomboidalis",
"Pseudocyttus_maculatus", "Pseudocyttus_maculatus", "Allocyttus_verrucosus",
"Allocyttus_verrucosus2", "Allocyttus_verrucosus3", "Allocyttus_folletti",
"Oreosoma_atlanticum", "Oreosoma_atlanticum2", "Oreosoma_atlanticum3",
"Capromimus_abbreviatus", "Capromimus_abbreviatus2", "Capromimus_abbreviatus3",
"Zenopsis_conchifer", "Zenopsis_conchifer2", "Zenopsis_nebulosa", "Zeus_faber",
"Zeus_faber2", "Zeus_capensis", "Cyttus_novaezealandiae", "Cyttus_novaezealandiae",
"Cyttus_australis", "Cyttus_traversi", "Stethopristes_eos", "Zenion_hololepis",
"Zenion_japonicus", "Zenion_japonicus", "Zenion_hololepis2", "Parazen_pacificus",
"Parazen_pacificus2", "Parazen_pacificus3", "Parazen_pacificus4", "Parazen_pacificus5",
```

```
"Xenolepidichthys_dalgleishi", "Xenolepidichthys_dalgleishi2",
"Grammicolepis_brachiusculus", "Grammicolepis_brachiusculus", "Cyttopsis_rosea",
"Cyttopsis_rosea2") )

gdftips<-as.vector(c( "Allocyttus_verrucosus", "Oreosoma_atlanticum",
"Capromimus_abbreviatus", "Zenopsis_conchifer", "Zeus_faber", "Cyttus_australis",
"Stethopristes_eos", "Zenion_hololepis", "Parazen_pacificus", "Xenolepidichthys_dalgleishi",
"Cyttopsis_rosea") ) #replaced all current tree tip labels with new names

tree<- drop.tip(tree, setdiff(tree$tip.label, gdftips))
plot(drop.tip(tree, setdiff(tree$tip.label, gdftips)))#drop tips not represented in data
plot(tree)

#WIREFRAME SECTION

gpacoords<-gpa1$coords

#FULL wireframe
wirevec<-
c(1,3,3,5,5,4,4,2,2,1,6,7,7,8,8,6,9,10,10,12,12,11,11,9,13,14,14,16,16,13,16,15,15,19,19,20,20,2
1,21,22,22,23,23,21,13,17,17,18,18,23)
wireframe <- matrix(wirevec, nrow=25, byrow=TRUE)
plotRefToTarget(gdf$coords[c(1,2,3,4,5,6,7,8,9,10,11,12,13,14,15,16,17,18,19,20,21,22,23),c(1,
2),which(PCA$x[,1]==min(PCA$x[,1]))],
gdf$coords[c(1,2,3,4,5,6,7,8,9,10,11,12,13,14,15,16,17,18,19,20,21,22,23),c(1,2),which(PCA$x[
,1]==max(PCA$x[,1]))], links=wireframe, method="points",mag=1)
```

```
plotRefToTarget(gdf$coords[c(1,2,3,4,5,6,7,8,9,10,11,12,13,14,15,16,17,18,19,20,21,22,23),c(1,
2),which(PCA$x[,2]==min(PCA$x[,2]))],
gdf$coords[c(1,2,3,4,5,6,7,8,9,10,11,12,13,14,15,16,17,18,19,20,21,22,23),c(1,2),which(PCA$x[
,2]==max(PCA$x[,2]))], links=wireframe, method="points",mag=1)
plotRefToTarget(gdf$coords[c(1,2,3,4,5,6,7,8,9,10,11,12,13,14,15,16,17,18,19,20,21,22,23),c(1,
2),which(PCA$x[,3]==min(PCA$x[,3]))],
gdf$coords[c(1,2,3,4,5,6,7,8,9,10,11,12,13,14,15,16,17,18,19,20,21,22,23),c(1,2),which(PCA$x[
,3]==max(PCA$x[,3]))], links=wireframe, method="points",mag=1)

#PREMAXILLA Wires (grey is the min/black is the max. whichever is first is grey)
wirevec<-c(1,3,3,5,5,4,4,2,2,1)
wireframe <- matrix(wirevec, nrow=5, byrow=TRUE)
plotRefToTarget(gdf$coords[c(1,2,3,4,5),c(1,2),which(PCA$x[,1]==min(PCA$x[,1]))],
gdf$coords[c(1,2,3,4,5),c(1,2),which(PCA$x[,1]==max(PCA$x[,1]))], links=wireframe,
method="points",mag=1)
plotRefToTarget(gdf$coords[c(1,2,3,4,5),c(1,2),which(PCA$x[,2]==min(PCA$x[,2]))],
gdf$coords[c(1,2,3,4,5),c(1,2),which(PCA$x[,2]==max(PCA$x[,2]))], links=wireframe,
method="points",mag=1)
plotRefToTarget(gdf$coords[c(1,2,3,4,5),c(1,2),which(PCA$x[,3]==min(PCA$x[,3]))],
gdf$coords[c(1,2,3,4,5),c(1,2),which(PCA$x[,3]==max(PCA$x[,3]))], links=wireframe,
method="points",mag=1)

#species level wireframe comparison!!!
plotRefToTarget(avverrucosus[c(1,2,3,4,5),c(1,2)], avdalgleishi[c(1,2,3,4,5),c(1,2)],
links=wireframe, method="points",mag=1)

#June 20, 2022
```

```
plot(avverrucosus[6:8,c(1,2)])
points(avdalgleishi[6:8,c(1,2)])

lines(wireframe[,1],wireframe[,2])
lines(wireframe[1,],wireframe[2,],col="black",lwd=1)
lines(wireframe)
wireframe[,1]
lines(avverrucosus[6:8,c(1,2)],avverrucosus[c(7,8,6),c(1,2)],col="black",lwd=1)
lines(c(avverrucosus[wireframe[,1],1],avverrucosus[wireframe[,2],1]),
    c(avverrucosus[wireframe[,1],2],avverrucosus[wireframe[,2],2]))
text(avverrucosus[6:8,c(1,2)], labels=c(6,7,8), cex=0.9, font=2)

plotRefToTarget(avverrucosus[c(1,2,3,4,5),c(1,2)], avdalgleishi[c(1,2,3,4,5),c(1,2)],
links=wireframe, method="points",mag=1)

#MAXILLA Wires
wirevec<-c(6,7,7,8,8,6)
wirevec<-c(1,2,2,3,3,1) #changed line just for 2D wireframe
wireframe <- matrix(wirevec, nrow=3, byrow=TRUE)
plotRefToTarget(gdf$coords[c(6,7,8),c(1,2),which(PCA$x[,1]==min(PCA$x[,1]))],
gdf$coords[c(6,7,8),c(1,2),which(PCA$x[,1]==max(PCA$x[,1]))], links=wireframe,
method="points",mag=1)
plotRefToTarget(gdf$coords[c(6,7,8),c(1,2),which(PCA$x[,2]==min(PCA$x[,2]))],
gdf$coords[c(6,7,8),c(1,2),which(PCA$x[,2]==max(PCA$x[,2]))], links=wireframe,
method="points",mag=1)
```

```
plotRefToTarget(gdf$coords[c(6,7,8),c(1,2),which(PCA$x[,3]==min(PCA$x[,3]))],
gdf$coords[c(6,7,8),c(1,2),which(PCA$x[,3]==max(PCA$x[,3]))], links=wireframe,
method="points",mag=1)

#DENTARY Wires
wirevec<-c(9,10,10,12,12,11,11,9)
wirevec<-c(1,2,2,4,4,3,3,1) #changed line just for 2D wireframe
wireframe <- matrix(wirevec, nrow=4, byrow=TRUE)
plotRefToTarget(gdf$coords[c(9,10,11,12),c(1,2),which(PCA$x[,1]==min(PCA$x[,1]))],
gdf$coords[c(9,10,11,12),c(1,2),which(PCA$x[,1]==max(PCA$x[,1]))], links=wireframe,
method="points",mag=1)
plotRefToTarget(gdf$coords[c(9,10,11,12),c(1,2),which(PCA$x[,2]==min(PCA$x[,2]))],
gdf$coords[c(9,10,11,12),c(1,2),which(PCA$x[,2]==max(PCA$x[,2]))], links=wireframe,
method="points",mag=1)
plotRefToTarget(gdf$coords[c(9,10,11,12),c(1,2),which(PCA$x[,3]==min(PCA$x[,3]))],
gdf$coords[c(9,10,11,12),c(1,2),which(PCA$x[,3]==max(PCA$x[,3]))], links=wireframe,
method="points",mag=1)

#ARTICULAR Wires
wirevec<-c(13,14,14,16,16,13)
wirevec<-c(1,2,2,3,3,1)
wireframe <- matrix(wirevec, nrow=3, byrow=TRUE)
plotRefToTarget(gdf$coords[c(13,14,16),c(1,2),which(PCA$x[,1]==min(PCA$x[,1]))],
gdf$coords[c(13,14,16),c(1,2),which(PCA$x[,1]==max(PCA$x[,1]))], links=wireframe,
method="points",mag=1)
```

```
plotRefToTarget(gdf$coords[c(13,14,16),c(1,2),which(PCA$x[,2]==min(PCA$x[,2]))],
gdf$coords[c(13,14,16),c(1,2),which(PCA$x[,2]==max(PCA$x[,2]))], links=wireframe,
method="points",mag=1)
plotRefToTarget(gdf$coords[c(13,14,16),c(1,2),which(PCA$x[,3]==min(PCA$x[,3]))],
gdf$coords[c(13,14,16),c(1,2),which(PCA$x[,3]==max(PCA$x[,3]))], links=wireframe,
method="points",mag=1)

#SYMPLECTIC Wires
wirevec<-c(19,20)
wirevec<-c(1,2)
wireframe <- matrix(wirevec, nrow=1, byrow=TRUE)
plotRefToTarget(gdf$coords[c(19,20),c(1,2),which(PCA$x[,1]==min(PCA$x[,1]))],
gdf$coords[c(19,20),c(1,2),which(PCA$x[,1]==max(PCA$x[,1]))], links=wireframe,
method="points",mag=1)
plotRefToTarget(gdf$coords[c(19,20),c(1,2),which(PCA$x[,2]==min(PCA$x[,2]))],
gdf$coords[c(19,20),c(1,2),which(PCA$x[,2]==max(PCA$x[,2]))], links=wireframe,
method="points",mag=1)
plotRefToTarget(gdf$coords[c(19,20),c(1,2),which(PCA$x[,3]==min(PCA$x[,3]))],
gdf$coords[c(19,20),c(1,2),which(PCA$x[,3]==max(PCA$x[,3]))], links=wireframe,
method="points",mag=1)
wireframe <- matrix(wirevec, nrow=3, byrow=TRUE)

#PREOPERCLE/JOINT Wires
wirevec<-c(13,17,17,18)
wirevec<-c(1,2,2,3)
wireframe <- matrix(wirevec, nrow=2, byrow=TRUE)
```

```
plotRefToTarget(gdf$coords[c(13,17,18),c(1,2),which(PCA$x[,1]==min(PCA$x[,1]))],
gdf$coords[c(13,17,18),c(1,2),which(PCA$x[,1]==max(PCA$x[,1]))], links=wireframe,
method="points",mag=1)
plotRefToTarget(gdf$coords[c(13,17,18),c(1,2),which(PCA$x[,2]==min(PCA$x[,2]))],
gdf$coords[c(13,17,18),c(1,2),which(PCA$x[,2]==max(PCA$x[,2]))], links=wireframe,
method="points",mag=1)
plotRefToTarget(gdf$coords[c(13,17,18),c(1,2),which(PCA$x[,3]==min(PCA$x[,3]))],
gdf$coords[c(13,17,18),c(1,2),which(PCA$x[,3]==max(PCA$x[,3]))], links=wireframe,
method="points",mag=1)

wireframe <- matrix(wirevec, nrow=3, byrow=TRUE)

#HYOMANDIBULA Wires
wirevec<-c(21,22,22,23,23,21)
wirevec<-c(1,2,2,3,3,1)
wireframe <- matrix(wirevec, nrow=3, byrow=TRUE)
plotRefToTarget(gdf$coords[c(21,22,23),c(1,2),which(PCA$x[,1]==min(PCA$x[,1]))],
gdf$coords[c(21,22,23),c(1,2),which(PCA$x[,1]==max(PCA$x[,1]))], links=wireframe,
method="points",mag=1)
plotRefToTarget(gdf$coords[c(13,17,18),c(1,2),which(PCA$x[,2]==min(PCA$x[,2]))],
gdf$coords[c(13,17,18),c(1,2),which(PCA$x[,2]==max(PCA$x[,2]))], links=wireframe,
method="points",mag=1)
plotRefToTarget(gdf$coords[c(13,17,18),c(1,2),which(PCA$x[,3]==min(PCA$x[,3]))],
gdf$coords[c(13,17,18),c(1,2),which(PCA$x[,3]==max(PCA$x[,3]))], links=wireframe,
method="points",mag=1)
wireframe <- matrix(wirevec, nrow=3, byrow=TRUE)
```

```
#connecting specific coordinates only, shows all coordinates
plotRefToTarget(gpacoords[,,10],gpacoords[,,20],links=wireframe, method="points",mag=1)
#wireframe works well

#PC1 MIN(grey) vs. PC1 MAX (black) = can use TPS, vector, points
#deformation grids - show next to PCAs
plotRefToTarget(gdf$coords[c(1,2,3,4,5),c(1,2),which(PCA$x[,1]==min(PCA$x[,1]))],
gdf$coords[c(1,2,3,4,5),c(1,2),which(PCA$x[,1]==max(PCA$x[,1]))], links=wireframe,
method="points",mag=1)
rgl.postscript('3dplot.pdf', fmt = 'pdf')
dev.copy2pdf(file="premaxilla wireframe.pdf")
dev.off()

#PC2 MIN vs. PC2 MAX
plotRefToTarget(gdf$coords[,,which(PCA$x[,2]==min(PCA$x[,2]))],
gdf$coords[,,which(PCA$x[,2]==max(PCA$x[,2]))], links=wireframe, method="points",mag=1)


#WIREFRAME GRAPH - change # depending on which connections we are observing
plot(gpacoords[,,1],asp=1)

for(i in 1:25){
  lines(
    gpacoords[wireframe[i,],1:3,1]
  )
```

REFERENCE LIST

Adams, D., M. Collyer, A. Kaliontzopoulou, and E. Baken. 2022. Geomorph: Software for geometric morphometric analyses. R package version 4.0.4. https://cran.r-project.org/package=geomorph.

Bellwood, D. R., Goatley, C. H. R., Cowman, P. F., & Bellwood, O. 2015. The evolution of fishes on coral reefs: Fossils, phylogenies, and functions. Ecology of Fishes on Coral Reefs, 55–63. https://doi.org/10.1017/cbo9781316105412.008

Stratovan Corporation. Stratovan Checkpoint [Software]. Version 2018.08.07. Aug 07, 2018. URL: https://www.stratovan.com/products/checkpoint

Baken, E., M. Collyer, A. Kaliontzopoulou, and D. Adams. 2021. geomorph v4.0 and gmShiny: enhanced analytics and a new graphical interface for a comprehensive morphometric experience.

Betancur-R., R., R. E. Broughton, E. O. Wiley, K. Carpenter, J. A. Lòpez, C. H. Li, N. I. Holcroft, D. Arcila, M. Sanciango, J. C. Cureton, II, F. F. Zhang, T. Buser, M. A. Campbell, J. A. Ballesteros, A. Roa-Varòn, S. Willis, W. C. Borden, T. Rowley, P. C. Reneau, D. J. Hough, G. Q. Lu, T. Grande, G. Arratia, and G. Ortí. 2013. The tree of life and a new classification of bony fishes. PLOS Currents Tree of Life: Apr 18. Edition 1. DOI: 10.1371/currents.tol.53ba26640df0ccaee75bb165c8c26288.

Boulenger, G. A. 1902. Pisces. In: Report on the collections of natural history made in the Antarctic regions during the voyage of the "Southern Cross". 344 p. Pt 5: 174–189, Pls. 11–18.

Borden, W. C., T. Grande, and W. L. Smith. 2013. Comparative osteology and myology of the caudal fin in the Paraccanthopterygii (Teleostei: Acanthomorpha), p. 419–455. In: Mesozoic Fishes 5–Global Diversity and Evolution. G. Arratia, H. P. Schultze, and M. V. H. Wilson (eds.). Verlag Dr. Friedrich Pfeil, München.

Chen, W.-J., Santini, F., Carnevale, G., Chen, J.-N., Liu, S.-H., Lavoué, S. Ã., & Mayden, R. L. 2014. New insights on early evolution of spiny-rayed fishes (Teleostei: Acanthomorpha). Frontiers in Marine Science, 1. https://doi.org/10.3389/fmars.2014.00053

Davesne, D., C. Gallut, V. Barriel, P. Janvier, G. Lecointre, and O. Otero. 2016. The phylogenetic interrelationships of spiny-rayed fishes (Acanthomorpha, Teleostei,

Actinopterygii): fossil taxa increase the congruence of morphology with molecular data. Frontiers in Ecology and Evolution 4: 1–20.

Davesne, D., G. Carnevale, and M. Friedman. 2017. *Bajaichthys elegans* from the Eocene of Bolca (Italy) and the overlooked morphological diversity of Zeiformes (Teleostei, Acanthomorpha). Paleontology 60: 255–268.

Duclos, K., T. Grande, and R. Cloutier. 2021. Evidence for modularity of the Weberian Apparatus in the zebrafish *Danio rerio* using micro-CT technology and 3-D geometric morphometrics. Verlag Pfeil. München. 59–70.

Foster, D. J., Podos, J., & Hendry, A. P. 2007. A geometric morphometric appraisal of beak shape in Darwin's finches. Journal of Evolutionary Biology, 21(1), 263–275. https://doi.org/10.1111/j.1420-9101.2007.01449.x

Ghezelayagh, A., R. C. Harrington, E. D. Burress, M. A. Campbell, J. C. Buckner, P. Chakrabarty, J. R. Glass, W. Tyler McCraney, P. J. Unmack, C. E. Thacker, M. E. Alfaro, S. T. Friedman, W. B. Ludt, P. F. Cowman, M. Friedman, S. A. Price, A. Dornburg, B. C. Faircloth, P. C. Wainwright, and T. J. Near. 2021. Prolonged morphological expansion of spiny-rayed fishes following the end-Cretaceous. Nature.

Grande, T., W. C. Borden, and W. L. Smith. 2013. Limits and relationships of Paracanthopterygii: a molecular framework for evaluating past morphological hypotheses, p. 385–418. In: Mesozoic Fishes 5–Global Diversity and Evolution. G. Arratia, H. P. Schultze, and M. V. H. Wilson (eds.). Verlag Dr. Friedrich Pfeil, München.

Grande, T. C., W. C. Borden, M. V. H. Wilson, and L. Scarpitta. 2018. Phylogenetic relationships among fishes in the order Zeiformes based on molecular and morphological data. Copeia 106 (1): 20–48.

Günther, A. 1860. Catalogue of the acanthopterygian fishes in the collection of the British Museum. Vol. 2. Squamipinnes, Cirrhitidae, Triglidae, Trachinidae, Sciaenidae, Polynemidae, Sphyraenidae, Trichiuridae, Scombridae, Carangidae, Xiphiidae. British Museum, London.

Heemstra, P. C. 1980. A revision of the zeid fishes (Zeiformes: Zeidae) of South Africa. Ichthyological Bulletin, J.L.B. Smith Institute of Ichthyology 41: 1–18.

Holt, E. W. L. 1894. Studies in teleostean morphology from the Marine Laboratory at Cleethorpes. Proceedings of the Zoological Society of London 1894, 413–446.

Hu, Y., L. Ghigliotti, M. Vacchi, E. Pisano, H. W. Detrich III, R. C. Albertson. 2016. Evolution in an extreme environment: developmental biases and phenotypic integration in the adaptive radiation of antarctic notothenioids. BMC Evolutionary Biology 16(1): 142.

Hughes, L. C., Ortí, G. (and 19 others). 2018. Comprehensive phylogeny of ray-finned fishes (Actinopterygii) based on transcriptomic and genomic data. Proceedings of the National Academy of Sciences. https://doi.org/10.1073/pnas.1719358115.

Johnson, G. D. and C. Patterson. 1993. Percomorph phylogeny: A survey and a new proposal. Bulletin of Marine Science 52: 554–626.

Fedorov, A., Beichel, R., Kalpathy-Cramer, J., Finet, J., Fillion-Robin, J.-C., Pujol, S., Bauer, C., Jennings, D., Fennessy, F., Sonka, M., Buatti, J., Aylward, S., Miller, J. V., Pieper, S., & Kikinis, R. 2012. 3D Slicer as an image computing platform for the Quantitative Imaging Network. Magnetic Resonance Imaging 30(9): 1323–1341. https://doi.org/10.1016/j.mri.2012.05.001

Klingenberg, C. P., & Marugán-Lobón, J. 2013. Evolutionary covariation in geometric morphometric data: Analyzing integration, modularity, and allometry in a phylogenetic context. Systematic Biology 62(4): 591–610. https://doi.org/10.1093/sysbio/syt025

Linnæus, C. 1758. Systema naturæ per regna tria naturæ, secundum classes, ordines, genera, species, cum characteribus, differentiis, synonymis, locis. Tomus I. Editio decima, reformata. 1–824. Holmiæ (Salvius).

Martin, C. H., and P. C. Wainwright. 2013. Multiple fitness peaks on the adaptive landscape drive adaptive radiation in the wild. Science 339: 208–211.

Near, T. J., R. I. Eytan, A. Dornburg, K. L. Kuhn, J. A. Moore, M. P. Davis, P. C. Wainwright, M. Friedman and W. L. Smith. 2012. Resolution of ray-finned fish phylogeny and timing of diversification. Proceedings of the National Academy of Sciences 109(34): 13698–13703.

Near, T. J., A. Dornburg, R. I. Eytan, B. P. Keck, W. L. Smith, K. L. Kuhn, J. A. Moore, S. A. Price, F. T. Burbrink, M. Freidman, P. C. Wainwright. 2013. Phylogeny and tempo of diversification in the superradiation of spiny-rayed fishes. Proceedings of the National Academy of Sciences 110(31): 12738–12743.

Nelson, J. S., T. C. Grande, and M. V. H. Wilson. 2016. Fishes of the World. Fifth Edition. John Wiley & Sons, Inc., New York.

Marcy, A. E., Fruciano, C., Phillips, M. J., Mardon, K., & Weisbecker, V. 2018. Low resolution scans can provide a sufficiently accurate, cost- and time-effective alternative to high resolution scans for 3D shape analyses. PeerJ, 6. https://doi.org/10.7717/peerj.5032

Miya, M., N. I. Holcroft, T. P. Satoh, M. Yamaguchi, M. Nishida, and E. O. Wiley. 2007. Mitochondrial genome and a nuclear gene indicate a novel phylogenetic position of deep-sea tube-eye fish (Stylephoridae). Ichthyological Research 54:323–332.

Parsons, K. J., Cooper, W. J., & Albertson, R. C. 2011. Modularity of the oral jaws is linked to repeated changes in the craniofacial shape of African cichlids. International Journal of Evolutionary Biology 641501: 1–10. https://doi.org/10.4061/2011/641501

Patterson, C. 1968. The caudal skeleton in Mesozoic acanthopterygian fishes. Bulletin of the British Museum (Natural History), Geology 17: 47–102.

Polly PD, Lawing AM, Fabre A, Goswami A. 2013. Phylogenetic principal components analysis and geometric morphometrics. Hystrix 24(1):1–9. doi:10.4404/hystrix-24.1-6383.

Regan, C. T. 1910. The anatomy and classification of the teleostan fishes of the order Zeomorphi. The Annals and Magazine of Natural History 8(6):481–484.

Revell, L. J. 2009. Size-correction and principal components for interspecific comparative studies. Evolution 63(12), 3258–3268. https://doi.org/10.1111/j.1558-5646.2009.00804.x

James Rohlf, F., and Marcus, L. F. 1993. A revolution in morphometrics. Trends in Ecology & Evolution 8(4): 129–132. https://doi.org/10.1016/0169-5347(93)90024-j

Rosen, D. E. 1984. Zeiforms as primitive plectognath fishes. American Museum Novitates 2782: 1–45.

Sáez, S., and J. Lamilla. 2017. Taxonomic update and illustrated key of Zeiformes from Chile (Pisces: Actinopterigii). Latin American Journal of Aquatic Research 45(1): 94–103.

Staab, K. L., R. Holzman, L. P. Hernandez, and P. C. Wainwright. 2012. Independently evolved upper jaw protrusion mechanisms show convergent hydrodynamic function in teleost fishes. Journal of Experimental Biology 215: 1456–1463.

Starks, E. C. 1898. The osteology and relationships of the family Zeidae. Proceedings of the United States National Museum 21: 469–476.

Tyler, J. C., B. O'Toole, and R. Winterbottom. 2003. Phylogeny of the genera and families of zeiform fishes, with comments on their relationships with tetraodontiforms and caproids. Smithsonian Contributions to Zoology 618: 1–110.

Tyler, J. C., and F. Santini. 2005. A phylogeny of the fossil and extant zeiform-like fishes, Upper Cretaceous to Recent, with comments on the putative zeomorph clade (Acanthomorpha). Zoologica Scripta 34: 157–175.

Westneat, M. W. 2004. Evolution of levers and linkages in the feeding mechanisms of fishes. Integrative and Comparative Biology 44(5): 378–389. https://doi.org/10.1093/icb/44.5.378

Wiley, E. O., G. D. Johnson, and W. W. Dimmick. 2000. The interrelationships of acanthomorph fishes: a total evidence approach using molecular and morphological data. Biochemical Systematics and Ecology 28: 319–350.

VITA

Jeffrey W. Peters was born in Morristown, New Jersey, on March 24, 1994. He graduated from Loyola University Chicago in May 2016 with a B.S. in Biology. During the summer of 2015, he was accepted into the Medical Summer Research Program at the Biomedical Research Institute of New Jersey where he presented research to scientists and physicians on Necrotizing Enterocolitis (NEC) that affects premature infants. Following that summer, as an undergraduate student he studied 2D geometric morphometrics and locality mapping of the order of fishes called Zeiformes in Dr. Terry Grande's lab. These early research opportunities introduced him to clinical medicine, evolution, and geometric morphometrics, which paved the way for an increased interest in fish morphology.

Upon completing his undergraduate degree, Mr. Peters continued research in Dr. Terry Grande's lab as he began pursuing his Master of Science at Loyola University Chicago, focusing on 3D jaw morphology of Zeiform fishes. He was able to present his graduate research at the American Society of Ichthyologists and Herpetologists (ASIH) during the summer of 2021. During his time at Loyola, he was also a Teaching Assistant in Dr. Grande's Comparative Anatomy lab course, as well as teaching as the Instructor of Record for the General Biology I and II lab courses. During the latter half of his graduate degree, Mr. Peters began working as an Optometric Technician at Solo Eyecare and Eyewear Gallery in Chicago. It was through both his clinical experience at Solo and his research background from Loyola that he decided to pursue a Doctor of Optometry degree from Illinois College of Optometry.